TRF2 binds branched DNA to safeguard telomere integrity

Isabelle Schmutz[1], Leonid Timashev[1], Wei Xie[2], Dinshaw J Patel[2] & Titia de Lange[1]

Although t-loops protect telomeres, they are at risk of cleavage by Holliday junction (HJ) resolvases if branch migration converts the three-way t-loop junction into four-way HJs. T-loop cleavage is repressed by the TRF2 basic domain, which binds three- and four-way junctions and protects HJs *in vitro*. By replacing the basic domain with bacterial-protein domains binding three- and four-way junctions, we demonstrated the *in vivo* relevance of branched-DNA binding. Branched-DNA binding also repressed PARP1, presumably by masking the PARP1 site in the t-loop junction. Although PARP1 recruits HJ resolvases and promotes t-loop cleavage, PARP1 activation alone did not result in t-loop cleavage, thus suggesting that the basic domain also prevents formation of HJs. Concordantly, removal of HJs by BLM helicase mitigated t-loop cleavage in response to loss of the basic domain. We propose that TRF2 masks and stabilizes the t-loop three-way junction, thereby protecting telomeres from detrimental deletions and PARP1 activation.

The six-subunit shelterin complex (composed of TRF1, TRF2, Rap1, TIN2, TPP1 and POT1)[1] is required to prevent telomeres from being recognized as sites of DNA damage[2,3]. Within shelterin, TRF2 is involved in the repression of two end-initiated DNA-damage-response pathways: the ATM kinase signaling pathway and nonhomologous end joining (NHEJ)[4–7]. TRF2 prevents ATM signaling and NHEJ by sequestering the chromosome end in the t-loop structure[8,9]. T-loops are formed through strand invasion of the single-stranded (ss) 3′ telomeric overhang into the double-stranded (ds) part of the telomere, thereby forming a three-way junction at the base of the t-loop (**Fig. 1a**).

Although t-loops are critical for telomere protection, they also are associated with two risks. First, the three-way junction at the base of the t-loop contains a recognition site for PARP1 (a recessed 5′ end[10–12]), whose activation can result in deleterious poly-ADP-ribosylation (PARsylation) of telomeric proteins. Second, branch migration of the base of the t-loop can generate a substrate for HJ resolvases. Whereas branch migration of the invasion point in one direction can evict the 3′ overhang and open the t-loop, branch migration in the opposite direction can lead to formation of a double HJ (dHJ) (**Fig. 1a**). If HJ resolvases process telomeric dHJs similarly to other HR intermediates, they could excise the loop and create large telomere truncations. Indeed, HJ resolvase–mediated excision of telomeric DNA occurs in cells expressing an allele of TRF2 (TRF2ΔB) resulting in the absence of the N-terminal 45–amino acid (aa) basic domain[13,14]. Although telomeres initially remain protected in cells expressing TRF2ΔB, telomere shortening due to repeated telomere truncations eventually leads to ATM signaling and senescence[5,7].

In vitro, the TRF2 basic domain has been shown to bind four-way (HJ) junctions irrespective of DNA sequence and to block their processing by HJ resolvases, thus suggesting that TRF2 protects telomeres from t-loop cleavage by simply masking HJs[15,16]. However, the basic domain has also been shown to interact with three-way junctions[15], the predicted structure at the base of the t-loop, thus raising the possibility that TRF2 may lock down the t-loop and subsequently prevent branch migration and dHJ formation. Despite the importance of the basic domain in telomere integrity, its mode of action *in vivo* remains unclear, and the relevance of the ability of TRF2 to bind three- and four-way junctions to the repression of t-loop cleavage has not been tested.

Here we establish that the basic domain of TRF2 functions *in vivo* as a domain that binds branched DNA. Our data showed that the basic domain of TRF2 has equal affinity for three- and four-way junctions and suggested that its interaction with the three-way junction at the base of the t-loop has a role in maintaining telomere integrity.

RESULTS

TRF2 binds three- and four-way junctions with the same affinity

TRF2 has previously been shown to bind to both three-way and four-way junctions[15,16], but the affinity for these binding substrates has not been compared side by side. To determine whether the basic domain has a preference for one of these binding substrates, we used surface plasmon resonance (SPR). Because TRF2 forms homodimers and homotetramers[7,17,18], thus possibly bringing multiple basic domains into apposition, we used a TRF2 fragment encompassing the TRFH dimerization domain and the basic domain (TRF2BH; **Fig. 1b**). This protein fragment lacked the C-terminal Myb domain, which binds double-stranded telomeric DNA, thus allowing us to prevent possibly confounding effects of nonspecific DNA interactions mediated by this domain. After gel filtration, purified recombinant TRF2BH showed a mass of 58.4 kDa, on the basis of multiangle static light scattering (MALS), thereby confirming its homodimerization (**Fig. 1c**).

[1]Laboratory for Cell Biology and Genetics, The Rockefeller University, New York, New York, USA. [2]Structural Biology Program, Memorial Sloan-Kettering Cancer Center, New York, New York, USA. Correspondence should be addressed to T.d.L. (delange@rockefeller.edu).

Received 5 April; accepted 11 July; published online 14 August 2017; doi:10.1038/nsmb.3451

The interaction analysis of TRF2BH with DNA ligands immobilized on sensor chips (**Fig. 1d**) revealed the expected preference of TRF2BH for branched DNA over dsDNA (**Fig. 1e**,**f**). The TRF2BH binding affinity for four-way-junction DNA (K_d of ~200 nM) was consistent with the affinity previously reported for four-way junctions[15]. Importantly, TRF2BH showed the same affinity for three-way junctions in multiple independent experiments (**Fig. 1g**), thus suggesting that the basic domain associates with the three-way junction at the base of the t-loop as well as with HJs that might be formed by branch migration.

The TRF2 basic domain does not affect t-loop frequency

Given its ability to associate with three-way junctions, we asked whether the basic domain might play a role in t-loop formation and/or maintenance. We applied super-resolution OMX-SI microscopy to spreads of DNA from psoralen- and UV-cross-linked nuclei[8] obtained from Cre-treated mouse embryonic fibroblasts (MEFs) expressing *lox*P-flanked *Terf2* (denoted *Trf2*$^{F/F}$ herein) and with *Lig4* knocked out (**Fig. 1h**). As expected from previous work[8], comparison of Cre-treated *Trf2*$^{F/F}$; *Lig4*$^{-/-}$ MEFs with cells complemented with wild-type TRF2 showed the dependence of t-loop formation on TRF2. Importantly, comparison of *Trf2*$^{F/F}$; *Lig4*$^{-/-}$ MEFs complemented with TRF2 or TRF2ΔB showed the same t-loop frequency after treatment with Cre (**Fig. 1i**,**j**), thus indicating that the basic domain is not required for t-loop formation and/or maintenance. Furthermore, the t-loop architecture was indistinguishable in the two settings (**Fig. 1k**). Although expression of TRF2ΔB induces t-loop cleavage and formation of t-circles, the imaging of telomere architecture applied here was unlikely to detect the rare circular DNAs induced by TRF2ΔB.

The presence of t-loops in cells expressing TRF2ΔB was consistent with the finding that the telomeres in these cells remained impervious to ATM signaling and NHEJ until they were extensively shortened by repeated t-loop cleavage. Because telomeres that have been extensively shortened cannot be visualized by our t-loop-imaging method, we did not analyze the effect of long-term expression of the TRF2ΔB allele on t-loop structure.

Branched-DNA binding is necessary for repression of t-loop cleavage

Although the *in vitro* data on the basic domain suggested that it may function as a branched DNA–binding domain *in vivo*, the possibility that its DNA binding features may be irrelevant to telomere protection could not be excluded. For instance, the basic domain may protect telomeres by interacting with a protein or a specific RNA. To determine whether branched-DNA binding by TRF2 is relevant to the protection of telomeres *in vivo*, we replaced the basic domain with bona fide branched DNA–binding domains. We chose branched DNA–binding domains from bacteria to exclude the possibility that they might share a protein or RNA interaction partner with the TRF2 basic domain. We focused on the branched DNA–binding domains from the *Escherichia coli* RuvABC HJ branch-migration and resolvase complex[19] (**Fig. 2a**). Like the basic domain, RuvC and RuvA bind to three- and four-way junctions with similar affinity[20–26].

The RuvC HJ resolvase ($RuvC_m$) and the DNA-binding domain of RuvA ($RuvA_{Nterm}$) were fused to the N terminus of TRF2ΔB (**Fig. 2a**) and expressed in mouse cells through retroviral transduction. These and other forms of TRF2 used in this study (**Supplementary Fig. 1a**) were expressed at levels approximately ten-fold greater than those of endogenous TRF2, thus resulting in replacement of the wild-type TRF2 by the exogenous alleles[7] (**Fig. 2b** and **Supplementary Fig. 1b**). Each version of TRF2 localized to telomeres (**Fig. 2c** and **Supplementary Fig. 1c**) and resulted in a two-fold increase in telomeric-DNA recovery in TRF2 chromatin immunoprecipitation (ChIP) assays (**Supplementary Fig. 1d**,**e**). Although TRF2 and TRF1 recognize the same DNA sequence, the wild-type and mutant forms of TRF2 did not displace TRF1 and appeared not to interfere with TRF1 function, because they did not induce the fragile-telomere phenotype indicative of compromised TRF1 (**Supplementary Fig. 1f**,**g** and refs. 27,28). The mutant forms of TRF2 fully complemented the phenotypes of TRF2 deletion in MEFs (**Supplementary Fig. 1h–j**), in agreement with previous findings that the basic domain of TRF2 is not required for repression of ATM signaling and NHEJ[5,7,14]. Furthermore, in complementation studies of *Trf2*$^{F/F}$; *Lig4*$^{-/-}$ cells, the expression of the $RuvC_m$-TRF2ΔB fusion protein yielded the same t-loop frequency as that of wild-type TRF2 (**Fig. 2d**).

To determine whether the RuvA and RuvC fusion proteins protected telomeres from t-loop cleavage, we assayed for the stochastic telomere truncations induced by this process. Postreplicative stochastic telomere truncations can be detected on the basis of unequal telomeric fluorescence *in situ* hybridization (FISH) signals of sister telomeres. We applied a quantitative FISH (Q-FISH) approach to determine the ratio of FISH signals of sister telomeres and to quantify the abundance of chromosome ends with unequal sister telomeres (Online Methods and **Supplementary Fig. 2a**). For each experimental condition, ~25–30 metaphases (from 3 or 4 independent experiments) were quantified, thus resulting in determination of the intensity ratios of >1,000 pairs of sister telomeres.

In the metaphases from control NIH3T3 cells and cells overexpressing wild-type TRF2, ~20% of the chromosome ends showed unequal sister telomeres according to our criteria (**Fig. 2e** and **Supplementary Fig. 2a**). As expected, the expression of TRF2ΔB significantly increased the frequency of unequal sister telomeres to 30–40%, thus indicating t-loop cleavage (**Fig. 2e** and **Supplementary Fig. 2a**). Fusion of either $RuvC_m$ or $RuvA_{Nterm}$ to TRF2ΔB restored the protection of telomeres, thereby resulting in chromosome ends with ~20% unequal sister telomeres (**Fig. 2e** and **Supplementary Fig. 2a**,**e**). Similarly, the $RuvC_m$ and $RuvA_{Nterm}$ fusion proteins restored the protection against the overall telomeric-DNA loss associated with t-loop cleavage, as determined by Q-FISH analysis and Southern blotting of telomeric restriction fragments (**Fig. 2f** and **Supplementary Fig. 2b–f**).

Similarly to mouse telomeres, human telomeres were protected from t-loop cleavage by the $RuvC_m$-TRF2ΔB fusion. When $RuvC_m$-TRF2ΔB was expressed in parallel with wild-type TRF2 and TRF2ΔB in HeLa cells (**Fig. 2g** and **Supplementary Fig. 3a–c**), TRF2ΔB induced stochastic telomere loss (evidenced by the higher frequency of unequal sister telomeres) whereas $RuvC_m$-TRF2ΔB did not (**Fig. 2h**). In addition, $RuvC_m$-TRF2ΔB rescued the total loss of telomeric DNA detected by Southern blotting and the formation of t-circles, as detected by 2D gel electrophoresis (**Fig. 2i**,**j**).

Finally, we tested the effect of a mutation in the TRF2 basic domain (H31A; **Supplementary Fig. 1a**) at a position that has previously been implicated in HJ binding[16]. This mutant behaved similarly to the TRF2ΔB allele and resulted in significant t-loop cleavage (**Fig. 2k–m** and **Supplementary Fig. 2g**,**h**). Collectively, the data showed that repression of t-loop cleavage by the basic domain of TRF2 involves its ability to bind to branched DNA.

The experiments with the $RuvC_m$-TRF2ΔB fusion protein used a RuvC mutant ($RuvC_m$)[29] that is catalytically inactive. Parallel experiments with wild-type RuvC ($RuvC_{WT}$) fused to TRF2ΔB showed the same protection against t-loop cleavage (**Supplementary Fig. 2c–f**), thus indicating that wild-type RuvC did not induce t-loop cleavage. The lack of t-loop cleavage by wild-type RuvC was most probably due to the

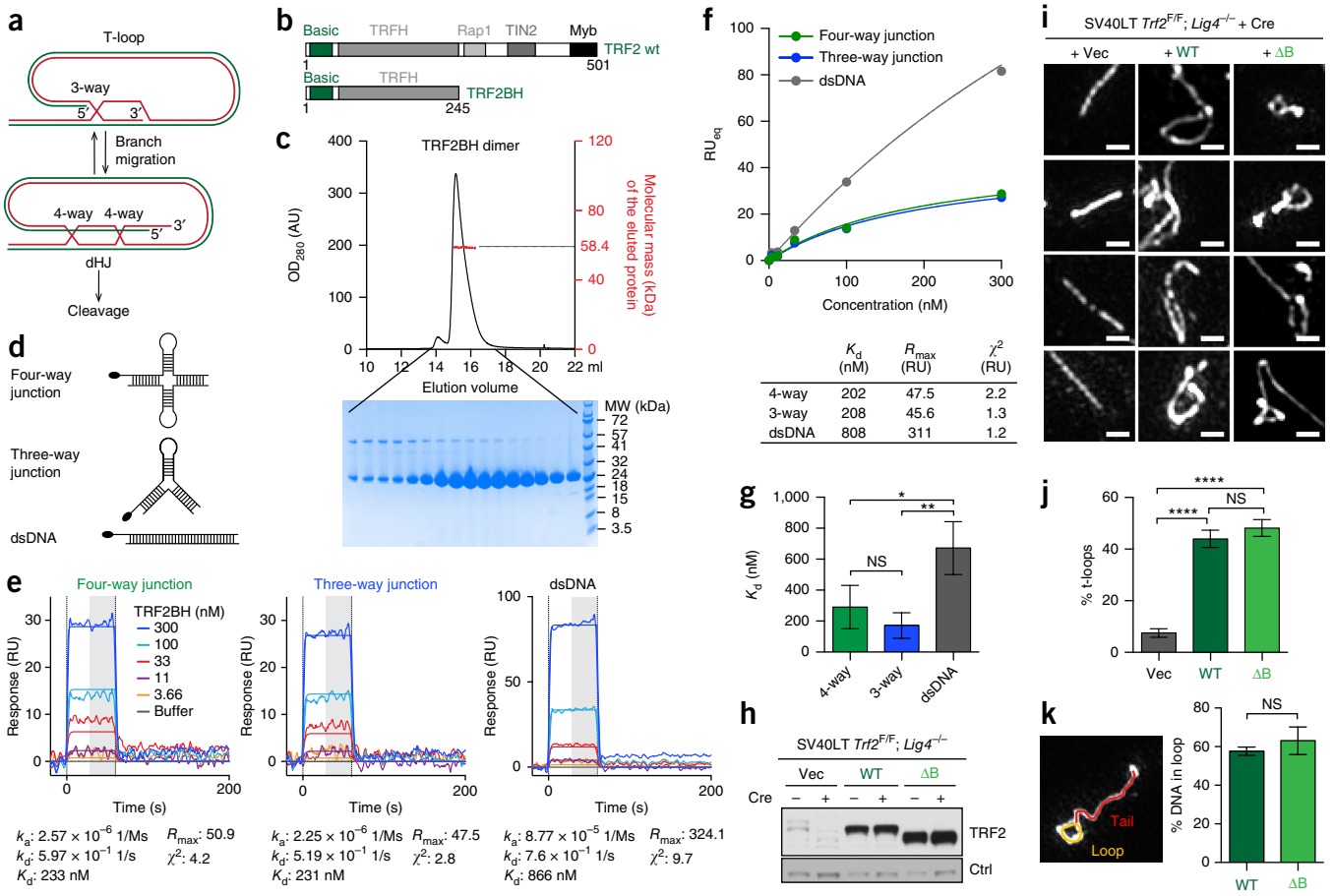

Figure 1 DNA binding and t-loop formation by the basic domain. (**a**) Schematic highlighting three- and four-way junctions at telomeres. (**b**) Schematic of wild-type (WT) TRF2 and $TRF2_{2–245}$ (TRF2BH). (**c**) Gel-filtration profile and Coomassie-stained SDS–PAGE gel showing purified TRF2BH. The red data points indicate molecular weight (MW) determinations by MALS of many of the fractions. TRF2BH has a mass of 58.4 kDa, thus indicating a dimer (right *y* axis). OD_{280}, optical density at 280 nm. (**d**) Schematic of the biotinylated-DNA ligands immobilized on the NeutrAvidin-coated surface of ProteOn NLC sensor chips. The ligands do not contain telomeric DNA. (**e**) SPR sensorgrams (representative of 3 total) of TRF2BH binding to the indicated substrates. Affinity kinetics was analyzed by the Langmuir 1:1 model fit on five serial dilutions of TRF2BH. The binding parameters are indicated. RU, response units. For dsDNA, the association constant k_a is lower. (**f**) SPR equilibrium analysis of the TRF2BH interaction with the indicated ligands, determined on the equilibrium part (gray) of the sensorgram in **e**. RU_{eq}, response units at equilibrium. With these TRF2BH concentrations, saturation was not reached for binding to dsDNA. (**g**) Mean K_d for TRF2BH binding to the indicated ligands (mean ± s.d.; $n = 3$ independent experiments). (**h**) TRF2 immunoblot for wild-type TRF2 and TRF2ΔB (ΔB) in infected $Trf2^{F/F}$; $Lig4^{-/-}$ MEFs. Ctrl, loading control (nonspecific band); vec, empty-vector control. SV40LT, SV40 large T antigen. (**i**) Representative OMX-SI super-resolution images of telomeres from Cre-treated $Trf2^{F/F}$; $Lig4^{-/-}$ cells complemented with wild-type TRF2, TRF2ΔB or vector. Scale bars, 0.5 µm. At least 300 molecules from 3 independent experiments were analyzed per experimental condition. (**j**) T-loop frequencies measured by OMX-SI super-resolution imaging of the cells shown in **i**. Mean ± s.d.; $n = 3$ independent experiments. (**k**) Analysis of percentage of telomeric DNA in the loop versus the loop plus tail (mean ± s.d.; $n = 3$ independent experiments). Significance was determined by one-way ANOVA with Tukey post test (**g**,**j**) or two-tailed unpaired *t* test (**k**). $****P < 0.0001$; $***P < 0.001$; $**P < 0.01$; $*P < 0.05$; NS, not significant.

absence of the preferred RuvC-cleavage site (5′-(A/T)TT↓(G/C)-3′, with downward arrow representing the cleavage site[30]) in telomeric DNA.

Branched-DNA binding by TRF2 represses PARP1

A recent report has suggested that the main mechanism by which the basic domain of TRF2 represses t-loop cleavage is through preventing PARP1 activation[31]. PARP1, one of the many DDR factors that are repressed by shelterin, has been inferred to become activated when shelterin is removed through deletion of TRF1 and TRF2 (refs. 32,33), presumably because telomeres lacking shelterin contain an exposed PARP1-activation site.

Repression of PARP1 by the shelterin complex was confirmed by detection of PARP1 through immunofluorescence (IF) combined with telomere FISH, thereby showing that PARP1 accumulated at telomeres devoid of all shelterin proteins (**Supplementary Fig. 4a**,**b**). We also detected a substantial increase in overall PARsylation in cells lacking shelterin at their telomeres (**Supplementary Fig. 4c**,**d**). In agreement with the view that PARP1 contributes to t-loop cleavage, PARP inhibition with olaparib or PARP1 gene deletion mitigated the TRF2ΔB-induced t-loop cleavage (**Fig. 3a-c** and **Supplementary Fig. 4e–g**).

Complementation of TRF2-deficient cells with wild-type TRF2 and TRF2ΔB confirmed the requirement of the basic domain of TRF2 in the repression of PARP1 accumulation at telomeres (**Fig. 3d–f**). Importantly, the repression of PARP1 was abolished by the H31A mutation in the basic domain (**Fig. 3d–f**) and was restored by fusion of $RuvC_m$ to TRF2ΔB (**Fig. 3d–f**). Thus, branched-DNA binding by the TRF2 basic domain is part of the mechanism by which PARP1 is repressed at telomeres and may potentially explain how TRF2 prevents t-loop cleavage. Within the t-loop structure, the PARP1-activation site

(a 5′ recessed end) is part of the three-way junction, thus suggesting that the binding of the TRF2 basic domain (as well as RuvC) to the three-way junction masks this site from PARP1 (**Fig. 3g**).

TRF2 and TIN2 repress PARP1 at telomeres

Given that the basic domain represses both PARP1 and t-loop cleavage, and considering the requirement for PARsylation in t-loop cleavage,

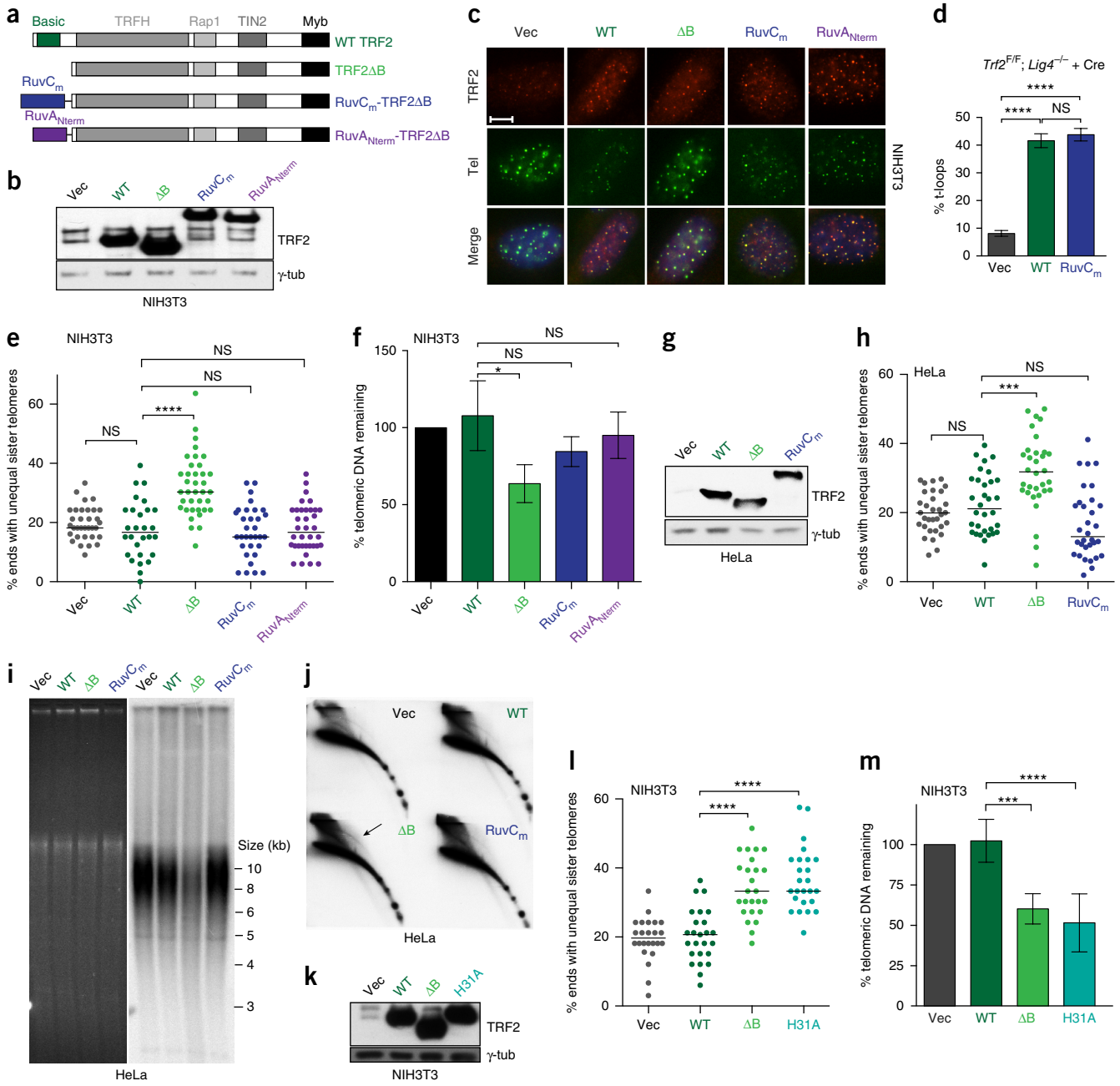

Figure 2 The basic domain functions as a branched DNA–binding domain *in vivo*. (**a**) Schematic of TRF2 alleles. (**b**) Immunoblot detecting wild-type TRF2 (WT), TRF2ΔB (ΔB) and $RuvC_m$- or RuvA-TRF2ΔB in infected NIH3T3 cells. γ-tub, γ-tubulin loading control. (**c**) IF–FISH for TRF2 (red) and telomere FISH (green). Blue, DAPI nuclear stain. Scale bar, 5 μm. Tel, telomere. (**d**) T-loop frequency in $Trf2^{F/F}$; $Lig4^{-/-}$ cells complemented with wild-type TRF2 and $RuvC_m$-TRF2ΔB (mean ± s.d.; $n = 3$ independent experiments). As in **Figure 1j**. (**e**) Quantification of chromosome ends with unequal sister telomeres (day 1 postinfection) in the NIH3T3 cells shown in **b**. Each data point represents the percentage of unequal sister telomeres in one metaphase spread. Bars, medians from ≥28 metaphases ($n = 4$ independent experiments). In each metaphase, 33–40 telomere pairs were analyzed, thus yielding a total of >1,000 chromosome ends analyzed per condition. (**f**) Q-FISH analysis of telomeric signal loss in NIH3T3 cells on day 5 postinfection (percentage telomeric DNA relative to the vector (vec)); mean ± s.d.; $n = 3$ independent experiments. (**g**) Immunoblot detecting hTRF2 alleles in infected HeLa1.2.11 cells. γ-tub, γ-tubulin loading control. (**h**) Unequal-sister-telomere assay as in **e** in the HeLa1.2.11 cells (day 8 postinfection) shown in **g**; median of ≥32 metaphases; $n = 3$ independent experiments. (**i**) Telomere blot of MboI/AluI-digested genomic DNA from the HeLa1.2.11 cells shown in **g**. Right, TTAGGG repeats; left, ethidium bromide staining confirming equal loading. (**j**) 2D gel analysis of the genomic DNA shown in **i**. Arrow, t-circle arc. (**k**) Immunoblot detecting wild-type TRF2, TRF2ΔB and TRF2H31A (H31A) in infected NIH3T3 cells. γ-tub, γ-tubulin loading control. (**l**) Unequal-sister-telomere assay as in **e** in the NIH3T3 cells shown in **k**; bars, medians from ≥25 metaphases; $n = 4$ independent experiments. (**m**) Q-FISH analysis of telomeric DNA signals as in **f** in NIH3T3 cells (day 5 postinfection); mean ± s.d.; $n = 5$ independent experiments. *P* values are based on one-way ANOVA with Tukey post test.

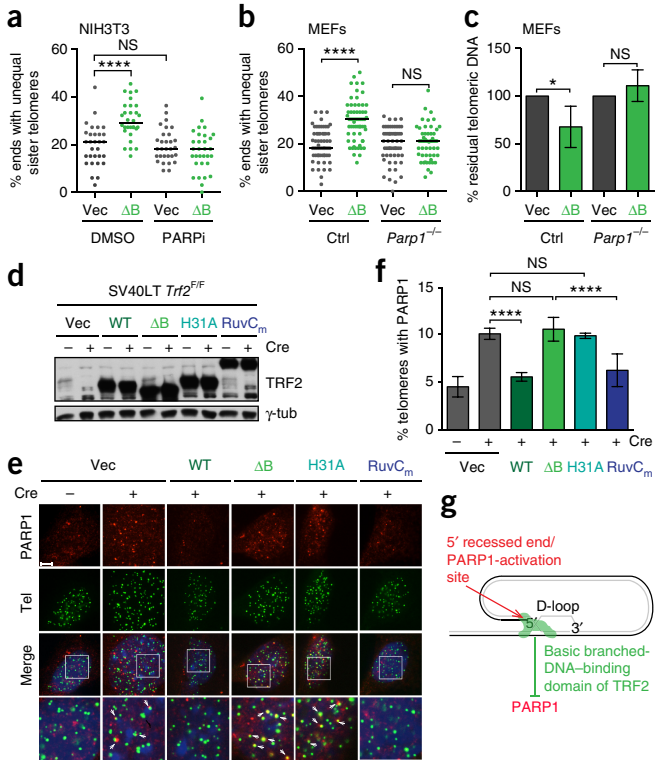

Figure 3 PARP1 promotes t-loop cleavage and is repressed by branched-DNA binding by TRF2. (**a**) Quantification of chromosome ends with unequal sister telomeres as in **Figure 2e** after treatment with DMSO (control) or PARP inhibitor (PARPi; 2 μM olaparib) in NIH3T3 cells infected with empty vector or TRF2ΔB (day 1 postinfection). Bars, medians from ≥30 metaphases (from $n = 3$ independent experiments). (**b**) Quantification of chromosome ends with unequal sister telomeres as in **Figure 2e** in control and *Parp1*$^{-/-}$ MEFs on day 1 postinfection. The data from two cell lines per genotype were pooled. (**c**) Q-FISH for telomeric DNA as in **Figure 2f**, using the cells in **b** on day 5 postinfection (mean ± s.d.; $n = 2$ independent experiments with two cell lines per genotype analyzed). (**d**) Immunoblot for the indicated *Trf2* alleles expressed in *Trf2*$^{F/F}$ cells. γ-tub, γ-tubulin loading control. (**e**) IF–FISH for PARP1 (red) at telomeres (green) in TRF2-deficient cells complemented with *Trf2* alleles as in **d**. Blue, DAPI nuclear stain. White arrows, PARP1 at telomeres. Scale bar, 5 μm. (**f**) Quantification of telomeres containing PARP1 in TRF2-deficient cells, performed as in **Supplementary Figure 4a,b**, using the cells in **d** (mean ± s.d.; $n = 3$ independent experiments). *P* values for all experiments based on one-way ANOVA with Tukey post test. (**g**) Schematic of the PARP1-activation site embedded in the three-way junction at the t-loop base and masking of this site by the TRF2 basic domain.

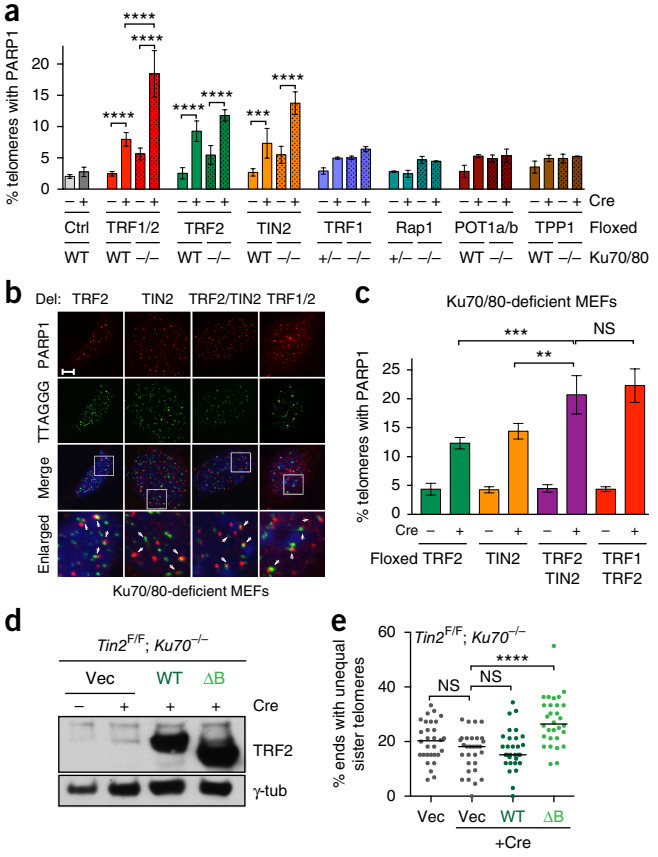

Figure 4 PARP1 activation is not sufficient to promote t-loop cleavage. (**a**) Quantification of telomeres containing PARP1, as in **Supplementary Figure 4a,b**. The graph represents mean ± s.d.; $n = 3$ independent experiments for Ctrl, TRF1, Rap1, POT1a/b and TPP1 floxed cells (Ku70/80-proficient and Ku70/80-deficient cells); $n = 6$ for TRF1/2 and TRF2 floxed cells (Ku70/80-proficient and Ku70/80-deficient cells); $n = 6$ for Ku70/80-proficient TIN2 cells; and $n = 8$ for Ku70/80-deficient TIN2 floxed cells. Not all genotypes were analyzed in the same experiment. Cre was expressed from a hit-and run retrovirus or from tamoxifen (4-OHT)-inducible *Rosa26-Cre-ERT2*. Ku deficiency denotes either Ku80 knockout or Ku70 knockout. MEFs were immortalized with SV40 large T antigen or were p53 deficient. (**b**) IF–FISH for PARP1 (red) at telomeres (green) in Ku-deficient *Trf1*$^{F/F}$; *Trf2*$^{F/F}$ MEFs and MEFs from littermate *Trf2*$^{F/F}$, *Tin2*$^{F/F}$ (official gene symbol *Tinf2*) or *Trf2*$^{F/F}$; *Tin2*$^{F/F}$ embryos. White arrows, PARP1 at telomeres. Blue, DAPI. Scale bar, 5 μm. (**c**) Quantification of telomeres containing PARP1 in MEFs as in **a**, using the cells in **b** (mean ± s.d.; n = from 3 independent experiments). (**d**) Immunoblot for the indicated *Trf2* alleles in *Tin2*$^{F/F}$; *Ku70*$^{-/-}$ cells. γ-tub, γ-tubulin loading control. (**e**) Quantification of chromosome ends with unequal sister telomeres as in **Figure 2e** in the *Tin2*$^{F/F}$; *Ku70*$^{-/-}$ cells shown in **d**. Cells were analyzed 96 h after deletion of *Tin2*. Bars, medians from ≥30 metaphases ($n = 2$ independent experiments). For all experiments, *P* values are based on one-way ANOVA with Tukey post test.

it is possible that PARP1 repression may be the main mechanism by which TRF2 protects telomeres from t-loop cleavage. To test this idea, we sought to activate PARP1 at telomeres in the presence of the basic domain (i.e., telomeres containing wild-type TRF2). If PARP1 activation at telomeres containing wild-type TRF2 was sufficient to allow for t-loop cleavage, the main function of the basic domain would appear to be repression of PARP1. Because the accumulation of PARP1 at telomeres lacking all shelterin subunits was greater than at telomeres lacking TRF2 (**Fig. 3f** and **Supplementary Fig. 4b**), we considered it likely that a second shelterin subunit might contribute to the repression of PARP1; hence, removal of the second subunit would allow us to test the role of PARP1 repression in protecting against t-loop cleavage. To identify this shelterin component, we performed a survey of conditional-knockout MEFs from which individual shelterin subunits were deleted (**Fig. 4a** and **Supplementary Fig. 5a**).

The shelterin-subunit deletions were performed in MEFs with or without the Ku70–Ku80 heterodimer, which is a general repressor of PARP1 (ref. 34). In agreement with its role as a general repressor of PARP1 binding to double-strand breaks, the Ku70–Ku80 heterodimer affected PARP1 localization to telomeres with compromised shelterin (**Fig. 4a**). The survey revealed that deletion of TIN2, but not Rap1, TRF1, TPP1 or POT1a and POT1b (POT1a/b), resulted in PARP1 accumulation at telomeres to the same extent as that observed after deletion of TRF2; in addition, the loss of TIN2 increased the overall PARsylation in the cells (**Fig. 4a–c** and **Supplementary Fig. 5a–c**).

The effect of TIN2 removal was specific and was not due to destabilization of TRF2, because overexpression of TRF2 did not diminish the accumulation of PARP1 (**Supplementary Fig. 5c–g**). Moreover, dual deletion of TIN2 and TRF2 resulted in a greater accumulation of PARP1 than did either deletion alone (**Fig. 4b**,**c** and **Supplementary Fig. 5b**), thus indicating that both proteins act independently. The PARP1 accumulation at telomeres lacking TRF2 and TIN2 was similar to that observed at telomeres lacking all shelterin components (**Fig. 4b**,**c** and **Supplementary Fig. 5b**), in agreement with the finding that the other shelterin subunits do not contribute to PARP1 repression.

Although telomeres lacking TIN2 showed PARP1 activation, the assay of unequal sister telomeres revealed no induction of t-loop cleavage (**Fig. 4d**,**e**). As a control, expression of TRF2ΔB in the TIN2-deficient cells resulted in the expected stochastic telomere losses indicative of t-loop cleavage (**Fig. 4d**,**e**). We concluded that PARP1 activation at telomeres is not sufficient to initiate t-loop cleavage. Furthermore, we inferred that TRF2 prevents t-loop cleavage in a manner that does not involve repression of PARP1, most probably by preventing branch migration and dHJ formation.

Rap1 has no role in repression of PARP1 or t-loop cleavage

Our survey of MEFs lacking individual shelterin subunits revealed that Rap1 does not contribute to PARP1 repression (**Fig. 4a**). It has recently been suggested that Rap1 (by cooperating with the TRF2 basic domain) can repress PARP1 and t-loop cleavage, thus leading to a striking loss of telomeres and induction of chromosome-end fusions when Rap1 and the TRF2 basic domain are simultaneously impaired[31]. To further analyze the potential role of Rap1 in protecting telomeres, we introduced TRF2ΔB and wild-type TRF2 into MEFs expressing *lox*P-flanked *Terf2ip* (denoted *Rap1*$^{F/F}$ herein) and determined the effect of Rap1 deletion on PARP1 accumulation at telomeres (**Supplementary Fig. 6a**,**b**). Deletion of Rap1 did not increase the TRF2ΔB-induced PARP1 accumulation at telomeres (**Supplementary Fig. 6a**,**b**). Furthermore, deletion of Rap1 did not exacerbate the telomere-loss phenotypes associated with TRF2ΔB expression even at later time points (**Supplementary Fig. 6c**,**d**), and there was no significant effect of Rap1 deletion on the formation of chromosome-end fusions (**Supplementary Fig. 6e**). Thus, using Cre-mediated gene deletion, we were unable to confirm a synergic role of Rap1 and the TRF2 basic domain in the preservation of telomere integrity. Two issues may underlie this discrepancy. First, we used Cre-mediated deletion (rather than Rap1-null cells), thus allowing comparison of isogenic sets of cells and avoiding changes resulting from long-term growth without Rap1. Second, our *Rap1*$^{F/F}$ cells lacked p53 and were therefore not subjected to immortalization with SV40 large T antigen, thus potentially affecting the outcomes of the experiments.

BLM diminishes TRF2ΔB-induced t-loop cleavage

The data above are consistent with a model in which the basic domain of TRF2 binds three-way junctions and consequently represses the two events leading to t-loop cleavage: the activation of PARP1 at the base of the t-loop and the branch migration that generates a dHJ. The latter proposed role of the basic domain predicts that dHJs are formed when the basic domain is impaired. If this hypothesis is correct, dissolution of dHJs should repress t-loop cleavage in response to TRF2ΔB. Because dissolution of dHJs relies on the BLM RecQ helicase[35], we determined the effect of BLM deficiency on t-loop cleavage. We used CRISPR–Cas9 gene editing to create BLM-deficient NIH3T3 cells (**Supplementary Fig. 7a**,**b**), which showed the expected increased sister-chromatid exchange (SCE) typical of BLM deficiency[35] (**Supplementary Fig. 7c**). We found that the absence of BLM significantly increased the levels of unequal-sister-telomere signals induced by TRF2ΔB (**Fig. 5a**,**b**). In agreement with this finding, the overall loss of telomeric DNA

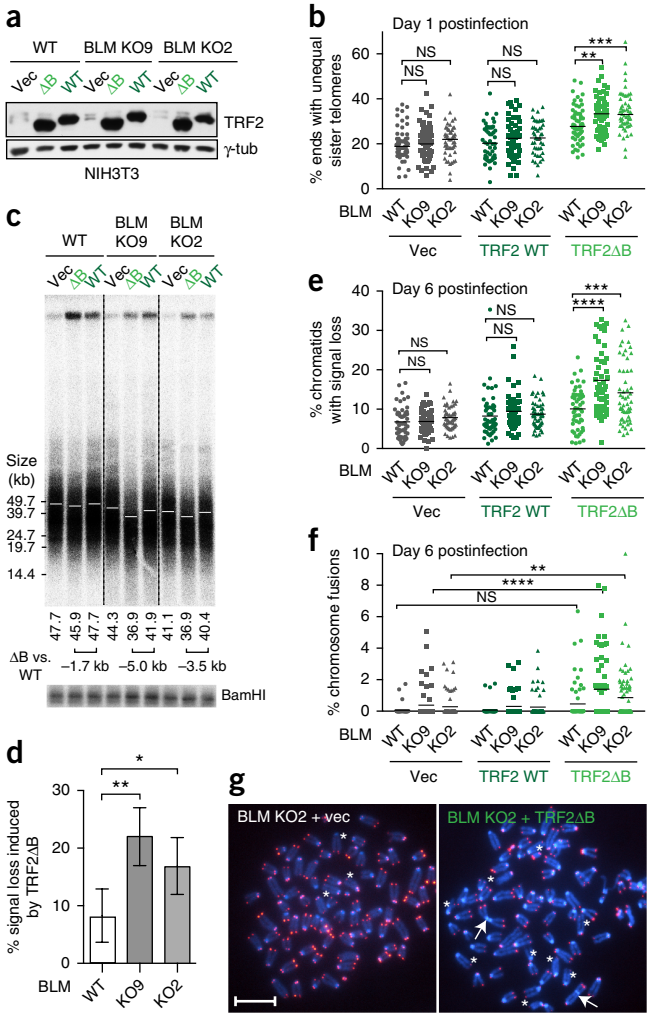

Figure 5 The role of branch migration in t-loop cleavage. (**a**) Immunoblot for TRF2 and γ-tubulin (loading control) in parental NIH3T3 cells and two independent BLM-deficient clones (KO9 and KO2) 1 d after infection. (**b**) Unequal-sister-telomere assay (as in **Fig. 2e**) in the cells shown in **a**. Bars, medians from ≥45 metaphases ($n = 4$ independent experiments, >1,500 chromosome ends). (**c**) Telomere blot analysis of MboI/AluI-digested DNA from parental and BLM-deficient NIH3T3 cells (as in **a** on day 6 after infection). Bottom, signal detected with the BamHI probe serving as loading control. White bars, median telomere lengths (values shown below the lanes). (**d**) TRF2ΔB-induced signal loss (mean ± s.d.; $n = 5$ experiments for KO2, and $n = 6$ experiments for WT and KO9 vector versus TRF2ΔB) calculated from telomere blots of MboI/AluI-digested DNA and normalized to the BamHI loading control as in **c**. (**e**) Quantification of chromatids showing loss of the telomere signal in parental and BLM-deficient NIH3T3 cells. Dots represent individual metaphase spreads, and the mean is shown (≥52 metaphase spreads from $n = 3$ independent experiments). (**f**) Quantification of chromosome fusions with no detectable telomere signals at the fusion sites in parental and BLM-deficient NIH3T3 cells. Dots represent the percentage of fused chromosomes in individual metaphase spreads, and the mean is shown (≥58 metaphase spreads from ≥ 58 metaphases from $n = 4$ independent experiments). (**g**) Representative metaphase spreads from vector-transduced and TRF2ΔB-expressing BLM KO2 cells showing chromosome fusions (white arrows) and signal-free chromatid ends (white asterisks). Scale bar, 10 μm. For **b**,**e** and **f**, *P* values are based on two-way ANOVA with Tukey post test; for **d**, *P* values are based on one-way ANOVA with Tukey post test. *P*-value symbols are as in **Figure 1**.

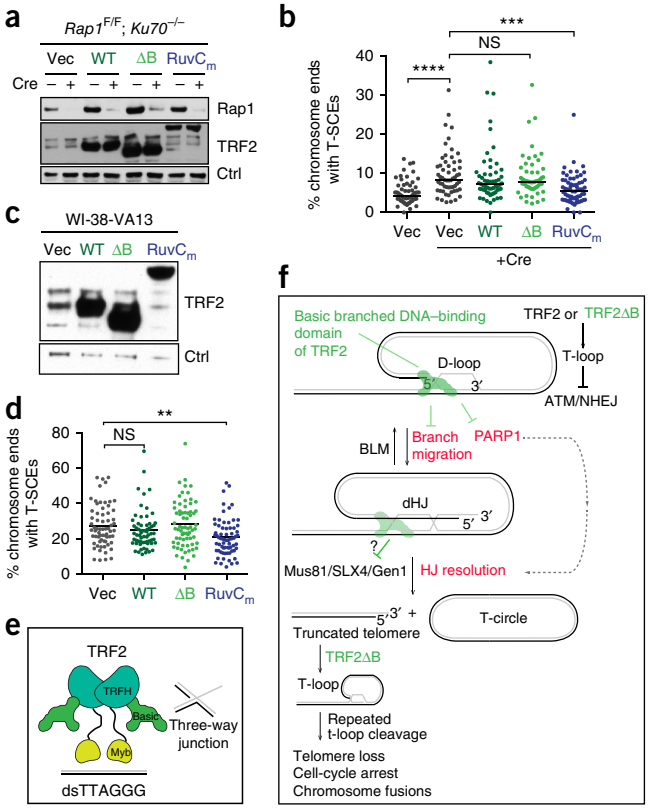

Figure 6 Repression of HR at telomeres by RuvC but not by the basic domain. (**a**) Immunoblot for TRF2 and Rap1 in *Rap1*$^{F/F}$; *Ku70*$^{-/-}$ MEFs analyzed 96 h after Cre treatment. Ctrl, loading control (nonspecific band). (**b**) Quantification of T-SCEs, as assessed by CO-FISH analysis in the cells shown in **a**. Data points from individual metaphase spreads are shown. Bars, means from ≥58 metaphases (3 independent experiments). (**c**) Immunoblot for hTRF2 in WI38-VA13 cells analyzed 7 d after introduction of TRF2 alleles. Ctrl, loading control (nonspecific band). (**d**) Quantification of T-SCEs in the cells shown in **c**. Data points from individual metaphase spreads are shown. Bars, means from ≥60 metaphases (n = 4 independent experiments). For all experiments, P values are based on one-way ANOVA with Tukey post test. (**e**,**f**) Schematic of TRF2 (**e**) and proposed mechanism for repression of t-loop cleavage and PARP1 activation by the basic domain (**f**). The branched DNA–binding domain can bind three- and four-way junctions. Three-way-junction binding by the basic domain is proposed to be critical for telomere protection, although a role of four-way binding is not excluded. Details in discussion.

induced by prolonged expression (6 d) of TRF2ΔB was elevated in BLM-deficient cells, and their telomeres appeared shorter (**Fig. 5c**,**d**). Similarly, the absence of BLM in cells expressing TRF2ΔB increased the frequency of chromatids lacking detectable telomere signals (**Fig. 5e**). Importantly, we did not detect any stochastic telomere deletions or telomere-signal loss in BLM-deficient NIH3T3 cells infected with empty vector or a vector for expression of wild-type TRF2 (**Fig. 5b**,**e**). This result was consistent with the lack of stochastic telomere truncations after Cre-mediated deletion of BLM in MEFs[36] and indicated that BLM deficiency does not induce t-loop cleavage when the telomeres contain wild-type TRF2. The BLM-mediated effect on t-loop cleavage in cells expressing TRF2ΔB was consistent with dHJs being formed and being the substrate for HJ resolvase–mediated t-loop cleavage. The TRF2 basic domain may potentially prevent formation of these dHJs through binding to the three-way junction and blocking branch migration.

Interestingly, when TRF2ΔB was expressed for 6 d, the BLM-deficient cells showed an increased frequency of chromosome fusions (**Fig. 5f**,**g**). These fusions were not observed 1 d after introduction of the TRF2ΔB allele (**Supplementary Fig. 7d**), thus indicating that TRF2ΔB-mediated telomere loss is progressive, and prolonged absence of the basic domain eventually results in telomeres that are too short to protect the chromosome ends from NHEJ.

RuvC but not the basic domain represses HR at telomeres

The data described above may be explained by the ability of the basic domain to bind three-way junctions. To determine whether the basic domain has HJ-binding activity *in vivo*, we sought to assay the effect of the basic domain (or its absence) on HR at telomeres. We hypothesized that HJ binding by the basic domain might allow TRF2 to repress HR-dependent formation of telomere sister-chromatid exchanges (T-SCEs), which can be detected by chromosome-orientation (CO) FISH. T-SCEs are induced after deletion of Rap1 from cells deficient in Ku70–Ku80 (ref. 37). If the basic domain binds HJs and blocks their resolution by HJ resolvases, as previously proposed[16], the frequency of T-SCEs would be expected to increase in *Rap1*$^{-/-}$ cells also deficient in *Xrcc6* (denoted *Ku70*$^{-/-}$ herein) and expressing TRF2ΔB. Expression of TRF2ΔB, compared with the vector control, did not increase the frequency of T-SCEs (**Fig. 6a**,**b**). Importantly, expression of RuvC$_m$-TRF2ΔB significantly decreased the level of T-SCEs, thus indicating that the presence of a genuine HJ-binding domain at telomeres can block HR (**Fig. 6a**,**b**). Overexpression of wild-type TRF2 resulted in a slight decrease in T-SCEs, but the effect was not significant. Similarly, the incidence of T-SCEs in the alternative lengthening of telomeres (ALT) cell line WI38-VA13 was diminished by RuvC$_m$-TRF2ΔB expression, whereas wild-type TRF2 and TRF2ΔB had no effect (**Fig. 6c**,**d**). The comparison of the effects of TRF2ΔB, RuvC$_m$-TRF2ΔB and wild-type TRF2 indicated that the basic domain of TRF2 was less proficient than RuvC in blocking HJ resolution.

DISCUSSION

Telomere protection by branched-DNA binding

The data reported here establish the mechanism by which the basic domain of TRF2 ensures that telomeres are not deleted by HJ resolvases and do not activate PARP1. Biochemical data have previously shown that the basic domain interacts *in vitro* with HJs and with three-way junctions[15,16]. The binding of the basic domain to HJs had been proposed to be its major mode of repression of t-loop cleavage[16]. However, our data suggested that the binding of the basic domain to the three-way branch point at the base of the t-loop is a major mechanism preserving telomere integrity.

The TRF2 basic domain binds with similar affinity (K_d of ~200 nM) to three- and four-way DNA junctions. The three-way junction tested here approximates the branch point at the base of the t-loop but lacks potentially important features (conformational flexibility, an ssDNA flap, a central 5′ end and telomeric sequences) that were not included for technical reasons. Further tests will be required to determine whether these features enhance the binding of the basic domain. Ultimately, structural information should reveal the exact DNA binding mode of the basic domain.

Replacement of the basic domain with RuvA and RuvC showed the importance of branched-DNA binding in both repression of t-loop cleavage and repression of PARP1. Because RuvA and RuvC bind to three- and four-way junctions, our experiments did not differentiate between these two modes of action. However, an important insight emerged from the repression of PARP1. In wild-type cells containing the basic domain at their telomeres, PARP1 was not activated despite

the presence of a PARP1-activation site at the branch point of the t-loop. This result suggested that the basic domain masks the PARP1-activation site by binding the three-way junction. The proposal that TRF2 acts by binding to three- but not four-way junctions is consistent with observations of HR at telomeres. We found no evidence indicating that the basic domain represses HR at telomeres, whereas $RuvC_m$ fused to TRF2 had this ability.

Three-way-junction binding by the basic domain can also explain how t-loop cleavage is repressed. If the binding of the basic domain to the t-loop branch point prevents branch migration, the dHJs that are the presumed substrate for HJ resolvases will not occur. The idea that the HJ resolvases act on dHJs that are formed when the basic domain is impaired was confirmed by the finding that BLM counteracts t-loop cleavage at telomeres deficient in the TRF2 basic domain.

A recent report has established that TRF2, via its basic domain, physically interacts with core histones and that this interaction is involved in the repression of t-loop cleavage[38]. *In vitro*, histone octamers have been shown to block spontaneous branch migration, probably by acting as a barrier[39]. This finding raises the possibility that the basic domain, when bound to the base of the t-loop, may interact with core histones and locally affect nucleosome stability or positioning. Such interactions, in addition to binding to the three-way junction, may contribute to the inhibition of branch migration by the basic domain.

We do not exclude an auxiliary role of HJ binding by the basic domain. However, the data obtained to date can be explained by the ability of this domain to bind to the three-way junction at the branch point of the t-loop. Remarkably, this association does not appear to be required for the formation or maintenance of t-loops.

The mechanism and consequences of t-loop cleavage

A detailed model for the events that lead to t-loop cleavage and its consequences can now be formulated (**Fig. 6e**,**f**). The t-loop is protected when it contains the TRF2 basic domain lodged on the three-way junction of the branch point. The presence of the basic domain at this site both masks the 5′ end of the telomere from recognition by PARP1 and stabilizes the three-way junction such that branch migration does not occur. In this protected state, the t-loop represses ATM kinase activation and NHEJ. When the basic domain is compromised (or absent), t-loops are still formed, but the branch point activates PARP1. PARsylation by PARP1 has been shown to result in recruitment of the SLX4–SLX1–Mus81 HJ resolvase[31,40]. This HJ resolvase may potentially cleave the three-way junction, but such processing would not result in deletion of telomeric DNA[41]. We propose that in the absence of the basic domain, the three-way junction is free to undergo branch migration, thus potentially forming a dHJ. Processing of the dHJ by HJ resolvases can then result in excision of the telomeric DNA in the loop. Resolution of the formed dHJs is counteracted by BLM, which is recruited to telomeres by TRF1 (ref. 42). Thus, the presence of the substrate for HJ resolvase–mediated t-loop cleavage is determined by the balance between branch migration in the t-loop and dHJ dissolution by BLM.

Initially, t-loop cleavage in cells with long telomeres would not show fewer t-loops, because TRF2ΔB can remodel the truncated telomere into a (smaller) t-loop. After repeated t-loop cleavage, excessive telomere shortening would ultimately result in one or more critically short telomeres that lack protection. At this stage, the ATM kinase would become activated, thus leading to senescence or apoptosis, and NHEJ would result in formation of end-to-end-fused chromosomes.

Interestingly, t-loop cleavage can occur spontaneously in cells expressing wild-type TRF2 (refs. 14,43–45). This process has been proposed to contribute to telomere-length regulation by trimming overelongated telomeres. An analogous pathway was originally discovered in budding yeast[46]. Recently, the telomere-associated protein TZAP has been shown to promote telomere trimming in ways that are not fully understood[47]. Because TRF2 readily displaces TZAP, TZAP presumably binds to only overelongated telomeres that are not fully coated with TRF2. It will be of interest to understand at which step TZAP promotes t-loop cleavage or whether it acts through a different pathway.

METHODS

Methods, including statements of data availability and any associated accession codes and references, are available in the online version of the paper.

Note: Any Supplementary Information and Source Data files are available in the online version of the paper.

ACKNOWLEDGMENTS

We thank D. White for expert mouse husbandry and the members of the laboratory of T.d.L. for sharing cell lines, for discussion and for comments on the manuscript. I.S. was supported by funds from a Women & Science Irene Diamond Fellowship in Breast Cancer Research at the Rockefeller University and by Mobility fellowships from the Swiss National Science foundation (Early Mobility fellowships PBFRP3-137230 and PBFRP3_142824, and Advanced Mobility fellowship P300PA_161006). L.T. was supported by an Anderson Center for Cancer Research Graduate Fellowship (contract FA9550-11-C-0028, awarded by the Department of Defense, Air Force Office of Scientific Research, National Defense Science and Engineering Graduate (NDSEG) Fellowship 32 CFR 168a). This work was supported by grants from the NIH (AG016642) to T.d.L. and (GM104962) to D.J.P., and by a Memorial Sloan-Kettering Cancer Center NIH Core Grant (P30 CA008748). T.d.L. is supported as an American Cancer Society Rose Zarucki Trust Research Professor. SPR experiments were performed at the RU High-Throughput and Spectroscopy Resource Center with expert assistance from A. Alcaino. OMX-SI imaging experiments were supported by a grant (S10RR031855) from the National Center For Research Resources to the Bio-Imaging Center at RU. The content of this manuscript is solely the responsibility of the authors and does not necessarily represent the official views of the National Center For Research Resources or the National Institutes of Health. We thank G. Hannon (Cancer Research UK Cambridge Institute) for reagents.

AUTHOR CONTRIBUTIONS

I.S. and T.d.L. designed the experiments and wrote the manuscript. I.S. performed all *in vivo* experiments, except for the t-loop assays, which were performed by L.T. W.X. and D.J.P. performed the *in vitro* binding studies.

COMPETING FINANCIAL INTERESTS

The authors declare no competing financial interests.

1. de Lange, T. Shelterin: the protein complex that shapes and safeguards human telomeres. *Genes Dev.* **19**, 2100–2110 (2005).
2. Lazzerini-Denchi, E. & Sfeir, A. Stop pulling my strings: what telomeres taught us about the DNA damage response. *Nat. Rev. Mol. Cell Biol.* **17**, 364–378 (2016).
3. Palm, W. & de Lange, T. How shelterin protects mammalian telomeres. *Annu. Rev. Genet.* **42**, 301–334 (2008).
4. Celli, G.B. & de Lange, T. DNA processing is not required for ATM-mediated telomere damage response after TRF2 deletion. *Nat. Cell Biol.* **7**, 712–718 (2005).
5. Karlseder, J., Broccoli, D., Dai, Y., Hardy, S. & de Lange, T. p53- and ATM-dependent apoptosis induced by telomeres lacking TRF2. *Science* **283**, 1321–1325 (1999).
6. Smogorzewska, A., Karlseder, J., Holtgreve-Grez, H., Jauch, A. & de Lange, T. DNA ligase IV-dependent NHEJ of deprotected mammalian telomeres in G1 and G2. *Curr. Biol.* **12**, 1635–1644 (2002).
7. van Steensel, B., Smogorzewska, A. & de Lange, T. TRF2 protects human telomeres from end-to-end fusions. *Cell* **92**, 401–413 (1998).
8. Doksani, Y., Wu, J.Y., de Lange, T. & Zhuang, X. Super-resolution fluorescence imaging of telomeres reveals TRF2-dependent T-loop formation. *Cell* **155**, 345–356 (2013).
9. Griffith, J.D. *et al.* Mammalian telomeres end in a large duplex loop. *Cell* **97**, 503–514 (1999).
10. Chasovskikh, S., Dimtchev, A., Smulson, M. & Dritschilo, A. DNA transitions induced by binding of PARP-1 to cruciform structures in supercoiled plasmids. *Cytometry A* **68**, 21–27 (2005).

11. Pion, E. *et al.* Poly(ADP-ribose) polymerase-1 dimerizes at a 5′ recessed DNA end *in vitro*: a fluorescence study. *Biochemistry* **42**, 12409–12417 (2003).
12. Potaman, V.N., Shlyakhtenko, L.S., Oussatcheva, E.A., Lyubchenko, Y.L. & Soldatenkov, V.A. Specific binding of poly(ADP-ribose) polymerase-1 to cruciform hairpins. *J. Mol. Biol.* **348**, 609–615 (2005).
13. Saint-Léger, A. *et al.* The basic N-terminal domain of TRF2 limits recombination endonuclease action at human telomeres. *Cell Cycle* **13**, 2469–2474 (2014).
14. Wang, R.C., Smogorzewska, A. & de Lange, T. Homologous recombination generates T-loop-sized deletions at human telomeres. *Cell* **119**, 355–368 (2004).
15. Fouché, N. *et al.* The basic domain of TRF2 directs binding to DNA junctions irrespective of the presence of TTAGGG repeats. *J. Biol. Chem.* **281**, 37486–37495 (2006).
16. Poulet, A. *et al.* TRF2 promotes, remodels and protects telomeric Holliday junctions. *EMBO J.* **28**, 641–651 (2009).
17. Bianchi, A., Smith, S., Chong, L., Elias, P. & de Lange, T. TRF1 is a dimer and bends telomeric DNA. *EMBO J.* **16**, 1785–1794 (1997).
18. Yoshimura, S.H., Maruyama, H., Ishikawa, F., Ohki, R. & Takeyasu, K. Molecular mechanisms of DNA end-loop formation by TRF2. *Genes Cells* **9**, 205–218 (2004).
19. Wyatt, H.D. & West, S.C. Holliday junction resolvases. *Cold Spring Harb. Perspect. Biol.* **6**, a023192 (2014).
20. Benson, F.E. & West, S.C. Substrate specificity of the *Escherichia coli* RuvC protein: resolution of three- and four-stranded recombination intermediates. *J. Biol. Chem.* **269**, 5195–5201 (1994).
21. Hiom, K. & West, S.C. Branch migration during homologous recombination: assembly of a RuvAB-Holliday junction complex *in vitro*. *Cell* **80**, 787–793 (1995).
22. Hiom, K., Tsaneva, I.R. & West, S.C. The directionality of RuvAB-mediated branch migration: *in vitro* studies with three-armed junctions. *Genes Cells* **1**, 443–451 (1996).
23. Iwasaki, H., Takahagi, M., Nakata, A. & Shinagawa, H. *Escherichia coli* RuvA and RuvB proteins specifically interact with Holliday junctions and promote branch migration. *Genes Dev.* **6**, 2214–2220 (1992).
24. Parsons, C.A. & West, S.C. Formation of a RuvAB-Holliday junction complex *in vitro*. *J. Mol. Biol.* **232**, 397–405 (1993).
25. Parsons, C.A., Stasiak, A., Bennett, R.J. & West, S.C. Structure of a multisubunit complex that promotes DNA branch migration. *Nature* **374**, 375–378 (1995).
26. Lloyd, R.G. & Sharples, G.J. Processing of recombination intermediates by the RecG and RuvAB proteins of *Escherichia coli*. *Nucleic Acids Res.* **21**, 1719–1725 (1993).
27. Sfeir, A. *et al.* Mammalian telomeres resemble fragile sites and require TRF1 for efficient replication. *Cell* **138**, 90–103 (2009).
28. Martínez, P. *et al.* Increased telomere fragility and fusions resulting from TRF1 deficiency lead to degenerative pathologies and increased cancer in mice. *Genes Dev.* **23**, 2060–2075 (2009).
29. Saito, A., Iwasaki, H., Ariyoshi, M., Morikawa, K. & Shinagawa, H. Identification of four acidic amino acids that constitute the catalytic center of the RuvC Holliday junction resolvase. *Proc. Natl. Acad. Sci. USA* **92**, 7470–7474 (1995).
30. Shah, R., Bennett, R.J. & West, S.C. Genetic recombination in *E. coli*: RuvC protein cleaves Holliday junctions at resolution hotspots *in vitro*. *Cell* **79**, 853–864 (1994).
31. Rai, R., Chen, Y., Lei, M. & Chang, S. TRF2-RAP1 is required to protect telomeres from engaging in homologous recombination-mediated deletions and fusions. *Nat. Commun.* **7**, 10881 (2016).
32. Mateos-Gomez, P.A. *et al.* Mammalian polymerase θ promotes alternative NHEJ and suppresses recombination. *Nature* **518**, 254–257 (2015).
33. Sfeir, A. & de Lange, T. Removal of shelterin reveals the telomere end-protection problem. *Science* **336**, 593–597 (2012).
34. Wang, M. *et al.* PARP-1 and Ku compete for repair of DNA double strand breaks by distinct NHEJ pathways. *Nucleic Acids Res.* **34**, 6170–6182 (2006).
35. Bizard, A.H. & Hickson, I.D. The dissolution of double Holliday junctions. *Cold Spring Harb. Perspect. Biol.* **6**, a016477 (2014).
36. Vannier, J.B., Pavicic-Kaltenbrunner, V., Petalcorin, M.I., Ding, H. & Boulton, S.J. RTEL1 dismantles T-loops and counteracts telomeric G4-DNA to maintain telomere integrity. *Cell* **149**, 795–806 (2012).
37. Sfeir, A., Kabir, S., van Overbeek, M., Celli, G.B. & de Lange, T. Loss of Rap1 induces telomere recombination in the absence of NHEJ or a DNA damage signal. *Science* **327**, 1657–1661 (2010).
38. Konishi, A., Izumi, T. & Shimizu, S. TRF2 protein interacts with core histones to stabilize chromosome ends. *J. Biol. Chem.* **291**, 20798–20810 (2016).
39. Grigoriev, M. & Hsieh, P. A histone octamer blocks branch migration of a Holliday junction. *Mol. Cell. Biol.* **17**, 7139–7150 (1997).
40. González-Prieto, R., Cuijpers, S.A., Luijsterburg, M.S., van Attikum, H. & Vertegaal, A.C. SUMOylation and PARylation cooperate to recruit and stabilize SLX4 at DNA damage sites. *EMBO Rep.* **16**, 512–519 (2015).
41. Doksani, Y. & de Lange, T. The role of double-strand break repair pathways at functional and dysfunctional telomeres. *Cold Spring Harb. Perspect. Biol.* **6**, a016576 (2014).
42. Zimmermann, M., Kibe, T., Kabir, S. & de Lange, T. TRF1 negotiates TTAGGG repeat-associated replication problems by recruiting the BLM helicase and the TPP1/POT1 repressor of ATR signaling. *Genes Dev.* **28**, 2477–2491 (2014).
43. Pickett, H.A., Cesare, A.J., Johnston, R.L., Neumann, A.A. & Reddel, R.R. Control of telomere length by a trimming mechanism that involves generation of t-circles. *EMBO J.* **28**, 799–809 (2009).
44. Pickett, H.A., Henson, J.D., Au, A.Y., Neumann, A.A. & Reddel, R.R. Normal mammalian cells negatively regulate telomere length by telomere trimming. *Hum. Mol. Genet.* **20**, 4684–4692 (2011).
45. Rivera, T., Haggblom, C., Cosconati, S. & Karlseder, J. A balance between elongation and trimming regulates telomere stability in stem cells. *Nat. Struct. Mol. Biol.* **24**, 30–39 (2017).
46. Li, B. & Lustig, A.J. A novel mechanism for telomere size control in *Saccharomyces cerevisiae*. *Genes Dev.* **10**, 1310–1326 (1996).
47. Li, J.S. *et al.* TZAP: a telomere-associated protein involved in telomere length control. *Science* **355**, 638–641 (2017).

ONLINE METHODS

Expression and purification of TRF2BH. The sequence corresponding to residues 2–245 of human TRF2 (named TRF2BH), synthesized by Genewiz, was inserted into a modified pRSFDuet-1 vector (Novagen) in which TRF2BH was fused to an N-terminal His_6-SUMO tag and expressed in *E. coli* BL21(DE3). The cells were cultured at 37 °C until an OD_{600} of approximately 0.8 was reached, then cooled to 18 °C and induced by addition of IPTG to the culture medium at a final concentration of 0.3 mM. After expression overnight, the cells were harvested by centrifugation at 4 °C and disrupted by sonication in buffer W (500 mM NaCl, 20 mM imidazole and 20 mM Tris-HCl, pH 8.0) supplemented with 1 mM PMSF protease inhibitor and 2 mM β-mercaptoethanol. After centrifugation, the supernatant was loaded onto an Ni–NTA affinity column. After extensive washing of the column with buffer W, TRF2BH was eluted with buffer W supplemented with 300 mM imidazole. The His_6-SUMO tag was removed by Ulp1 protease during dialysis against buffer containing 20 mM Tris-HCl, 200 mM NaCl and 1 mM DTT, pH 7.5. After dialysis, the protein sample was further fractionated over a heparin column, then subjected to gel filtration on a 16/60 G200 Superdex column (GE Healthcare) with buffer G (150 mM NaCl, 20 mM Tris-HCl, pH 7.5, and 1 mM DTT).

Oligonucleotide annealing. All oligonucleotides were purchased from IDT. To make the immobile four-way DNA junction, primer432 and primer4 were annealed at a 1:1 molar ratio. To make the three-way immobile DNA junction, primer432 and primer 3 were annealed at a 1:1 molar ratio. To make the dsDNA, primer432 and primer 2 were annealed at a 1:1 molar ratio.

primer432, 5′-biotin-TTTTTTTTTCAATCGGCTTTGACCTTTGGTC AATCGGCAGAT-3′
primer4, 5′-ATCTGCCGATTCTGGTTTCCAGAAAGCCGATTG-3′
primer3, 5′-ATCTGCCGAAGCCGATTG-3′
primer2, 5′-ATCTGCCGATTGACCAAAGGTCAAAGCCGATTG-3′

Surface plasmon resonance (SPR). Binding analysis was carried out on a 6 × 6 multiplex ProteOn XPR36 System (Bio-Rad) at 25 °C. Annealed oligonucleotides were diluted in buffer (10 mM HEPES, pH 7.3, and 200 mM NaCl) to a final concentration of 5 nM and were passed over a ProteOn NLC (NeutrAvidin-coated) sensor chip for immobilization (50–300 response units (RU) with the same buffer). The protein was diluted in the same buffer supplemented with BSA and Tween-20 (10 mM HEPES, pH 7.2, 200 mM NaCl, 0.05% Tween-20 and 1 mg/ml BSA), and serial dilutions were injected in BSA-supplemented buffer over the DNA-coated sensor chip at a flow rate of 100 µl/min for 60 s and were subsequently allowed to dissociate for 200 s. The chip surface was regenerated by sequential injections of 0.1% SDS and 1 M NaCl at a flow rate of 100 µl/min for 30 s each. All interactions were measured simultaneously. Reproducibility was verified with two additional experiments performed on independent chips.

Analysis of the data was performed with ProteOn XPR36 Manager software (BioRad) on reference-subtracted sensorgrams. Channel referencing was performed on baseline-subtracted data by subtraction of the reference channel (surface with no immobilized DNA ligand) and double referencing with the interaction data from a blank sample (buffer) injected simultaneously with the serial protein dilutions. Equilibrium (dissociation constant, K_d) and kinetic (rate constants, k_a and k_d) parameters for the binding of TRF2BH to different DNA ligands were determined by fitting the 1:1 Langmuir binding model, which describes a 1:1 interaction between one ligand molecule and one analyte molecule, to the data.

Expression vectors. pLPCpuro was used as the retroviral expression vector for mouse and human TRF2 alleles. pLPC-hTRF2 and pLPC-hTRF2ΔB were as previously described[48]. pLPC-mTRF2 and pLPC-mTRF2ΔB were generated accordingly with mouse TRF2 cDNA[49]. mTRF2-H31A was generated by site-directed mutagenesis and cloned into pLPCpuro-NMyc. The $RuvC_{wt}$-mTRF2ΔB expression vector was generated by cloning the *E. coli* RuvC cDNA[50] (Addgene) upstream of the TRF2ΔB cDNA with a GSGGSGGGSGGS linker (12 aa). Site-directed mutagenesis was used to introduce D138N and D140N mutations into RuvC for the generation of $RuvC_m$-mTRF2ΔB. The $RuvA_{N\text{-}term}$-mTRF2ΔB expression vector was generated by cloning the *E. coli* RuvA cDNA (Ensembl Bacteria, b1861, cDNA synthesized by Genewiz) upstream of the TRF2ΔB cDNA with the 12-aa (GSGGSGGGSGGS) linker and using overlap-extension PCR to delete the 56-aa C-terminal fragment of RuvA (aa 147–203) containing the RuvB-binding site (primers fw1, 5′-GGCTTATCGAAATTAATACG-3′; rv1, 5′-ACCACCGGATCCGAGTACCAGGTCGGC-3′; fw2, 5′-GACCTGGTACTC GGATCCGGTGGTTCT-3′; and rv2, 5′-CCTCATTGTACTTGAAGCAGC-3′). For expression of $RuvC_m$-hTRF2ΔB in human cells, the mutated RuvC cDNA was cloned upstream of the hTRF2ΔB cDNA by using a GSGGSGGGSGGS linker. pWZLhygro-NMyc was used as retroviral expression vector for the experiments in **Supplementary Figure 5c–g**.

Cell culture. *Trf2*$^{F/F}$, *Tin2*$^{F/F}$, *Trf1*$^{F/F}$, *Rap1*$^{F/F}$, *Tpp1*$^{F/F}$, *Pot1a*$^{F/F}$, *Pot1b*$^{F/F}$, *Cre-ERT2*, *Ku70*$^{-/-}$, *Ku80*$^{-/-}$ (official symbol *Xrcc5*) *Lig4*$^{-/-}$ and p53$^{-/-}$ (official symbol *Trp53*) mice were as described previously[4,27,37,51–58]. *Parp1*^{tm1Zqw} mice (002779, Jackson Laboratory) were intercrossed with C57BL/6J to obtain controls (*Parp1*$^{+/+}$ and *Parp1*$^{+/tm1Zqw}$ cell lines). Compound genotypes were obtained by intercrossing, and MEFs were isolated from embryonic day (E) 12.5 or E 13.5 embryos through standard techniques. Animal work was executed at the Rockefeller University's Comparative Bioscience Center according to NIH guidelines under protocol 16865-H *Trf2*$^{F/F}$, *Trf2*$^{F/F}$; *Ku70*$^{-/-}$, *Trf2*$^{F/F}$; *Lig4*$^{-/-}$, *Tin2*$^{F/F}$, *Tin2*$^{F/F}$; *Ku70*$^{-/-}$, *Trf2*$^{F/F}$; *Tin2*$^{F/F}$; *Ku70*$^{-/-}$, *Tpp1*$^{F/F}$, *Tpp1*$^{F/F}$; *Ku70*$^{-/-}$, *Pot1a/b*$^{F/F}$, *Pot1a/b*$^{F/F}$; *Ku70*$^{-/-}$, *Parp1* control and *Parp1*$^{-/-}$ MEFs were immortalized with SV40 large T antigen. *Trf1*$^{F/F}$; *Ku80*$^{+/-}$, *Trf1*$^{F/F}$; *Ku80*$^{-/-}$, *Rap1*$^{F/F}$; *Ku70*$^{+/-}$, *Rap1*$^{F/F}$; *Ku70*$^{-/-}$, *Trf1*$^{F/F}$; *Trf2*$^{F/F}$ and *Trf1*$^{F/F}$; *Trf2*$^{F/F}$; *Ku80*$^{-/-}$ MEFs were *p53*$^{-/-}$. For SV40 large T antigen immortalization, primary MEFs were immortalized at PD1 or PD2 by two consecutive retroviral infections with pBabe-SV40LT (a gift from G. Hannon) and cultured in DMEM (Gibco) supplemented with 15% FBS (Gibco), 2 mM L-glutamine, 100 U/ml penicillin (Sigma), 0.1 mg/ml streptomycin (Sigma), 0.1 mM nonessential amino acids (Invitrogen), 1 mM sodium pyruvate (Sigma) and 50 mM β-mercaptoethanol (Chemicon). Genotyping was performed by Transnetyx through real-time PCR with allele-specific probes.

Mouse NIH3T3 (ATCC); human HeLa1.2.11 (ref. 7), Hela1.3 (ref. 59), 293T (ATCC); and Phoenix virus packaging (ATCC) cell lines were grown in DMEM supplemented with 10% bovine calf serum (Hyclone), 2 mM L-glutamine, 100 U/ml penicillin, 0.1 mg/ml streptomycin, and 0.1 mM nonessential amino acids. WI-38-VA13 cells were grown in the same medium but supplemented with 15% FBS (Gibco). PARP inhibitor (olaparib, AZD2281, Selleck Chemicals) was dissolved in DMSO and added at a final concentration 5 or 2 µM. All cell lines used were tested for mycoplasma. Human cell lines were authenticated.

For CRISPR–Cas9 genomic editing, the guide sequence was determined by ZiFit (http://zifit.partners.org/) as sgBLM, 5′-GCTGTATGCGTATCTGC-(PAM)-3′. Oligonucleotides were purchased from Sigma-Aldrich and cloned into the AflII-digested gRNA-expression vector (Addgene) by Gibson assembly (NEB). The expression vectors for gRNA and hCas9 (Addgene) were introduced by electroporation with a Kit R Nucleofector Kit (Lonza). Single-cell clones isolated with limiting dilution were screened by immunoblotting, and DNA sequencing with TOPO-cloned PCR products (Invitrogen) was performed to verify genomic editing (Blm_fw, 5′-TTTCCTCATGTCTTCCTCCTG-3; Blm_rv, 5′- TGAAGAAAGAAAGCACAATAAATATGA-3′).

Retroviral and lentiviral infections. For retroviral infections, 4×10^6 to 5×10^6 Phoenix ecotropic or amphotropic packaging cells were plated 24 h before transfection. Cells were transfected with 20 µg of the desired plasmid with calcium-phosphate coprecipitation and provided with fresh medium twice, 12–16 h and 24–30 h after transfection. At 48 h after transfection, virus-containing medium was filtered through a 45-µm filter, then supplemented with 4 µg/ml polybrene and used for infection of target cells. The medium of the packaging cells was replenished and used for later infections. For expression of exogenous alleles, two or three infections in 12-h intervals were applied. 12 h after the last infection, cells were provided with fresh medium and plated in selective medium containing appropriate antibiotics (0.6–2.5 µg puromycin or 135 µg/ml hygromycin) 24 h after the last infection. Selection was maintained until all the cells in an uninfected control had died. For the harvest of NIH3T3 cells on day 1 postinfection, cells were plated 12 h after the last infection.

For introduction of shRNA against PARP1, 4.5×10^6 293T cells were plated 24 h before transfection with 20 µg shRNA plasmid (pLK0.1, GGCCCTTGGAAACATGTATG[33], and packaging vectors using calcium phosphate coprecipitation. Four infections in 12-h intervals over 2 d were used. 12 h after the last infection, cells were plated into selective medium.

doi:10.1038/nsmb.3451

Cre recombinase was introduced into MEFs by three consecutive infections in 12-h intervals with a pMMP Hit&Run Cre retrovirus without subsequent antibiotic selection. For infection, 0.5×10^6 MEFs were plated 24 h before infection. Experimental time points were counted starting 12 h after the first infection. Cells were plated for harvest at $t = 24$ h, medium was changed at $t = 72$ h, and cells were harvested at 96 h. For the *Rosa26-Cre-ERT2* inducible cell lines, Cre expression was induced by treatment with 1 μM 4-OH tamoxifen (4-OHT) in the growth medium. The medium was exchanged 8 h after 4-OHT addition, and cells were plated for harvest 24 h after induction. The time point of 4OHT addition was set as $t = 0$ h. Efficient deletion of the floxed alleles was verified by immunoblotting and (where appropriate) monitoring telomere-dysfunction-induced foci.

T-loop assay. Cells were spread for t-loop imaging as previously described[8]. Briefly, cells were lysed in fibroblast lysis buffer (12.5 mM Tris, pH 7.4, 5 mM KCl, 0.1 mM spermine, 0.25 mM spermidine and 175 mM sucrose, supplemented with protease-inhibitor cocktail (Roche)), and nuclei were spun down at 1,000*g* for 5 min and washed in nuclei wash buffer (10 mM Tris-HCl, pH 7.4, 15 mM NaCl, 60 mM KCl, 5 mM EDTA and 300 mM sucrose). Nuclei were cross-linked three times with 100 μg/ml trioxsalen under 365-nm light, then washed in nuclei wash buffer. Subsequently, nuclei were lysed with spreading buffer (10 mM Tris-HCl, pH 7.4, 10 mM EDTA, 0.05% SDS and 1 M NaCl), and the DNA was cytospun onto coverslips. The standard FISH procedure was used to hybridize a triple-TTAGGG-Cy3 (TelG-Cy3) PNA probe, and DNA spreads were then imaged on a GE OMX V4 microscope. At least 100 countable molecules were scored per sample per experiment. Countable molecules were split into two categories: linear (continuous straight molecules that did not have any branches and were uniformly dense) and loops (molecules with a continuous, hollow loop at one end). Molecules that could not be classified as either linear or loops were discarded from the analysis.

Immunoblotting. Whole cell lysates were prepared by lysis of cells in buffer C (20 mM HEPES-KOH, pH 7.9, 0.42 M KCl, 25% glycerol, 0.1 mM EDTA, 5 mM $MgCl_2$, 0.2% NP-40 and complete protease-inhibitor cocktail), and immunoblotting was performed as described previously[4]. Lysate equivalent to 10^5 cells was resolved with SDS–PAGE and transferred to a nitrocellulose membrane. Antibodies to the following proteins were used: rabbit mTRF2 (cat. no.1254), rabbit hTRF2 (cat. no. 647), rabbit BLM (Abcam, Ab2179), mouse γ-tubulin (Sigma GTU88), mouse PAR (Trevigen, 4335-MC), rabbit mTRF1 (cat. no. 1449), rabbit mTIN2 (cat. no. 1447), rabbit mRap1 (cat. no.1252), rabbit mPot1a (cat. no. 1221), rabbit mPot1b (cat. no. 1223) and mouse c-Myc 9E10 (Calbiochem). Immunoblotting for POT1a and POT1b was performed with a previously described renaturation protocol[53]. Uncropped immunoblot images of key data are shown in **Supplementary Data Set 1**.

IF–FISH. Cells grown on coverslips to subconfluence were fixed in MeOH for 10 min at −20 °C. IF and IF–FISH were carried out as previously described[60]. For FISH, a FITC-OO-$(CCCTAA)_3$ PNA probe (PNA Bio) was used. Images were captured with a Zeiss Axioplan II microscope equipped with a Hamamatsu C4742-95 camera and controlled by Volocity software (GE Healthcare). Antibodies to the following proteins were used for IF: rabbit mTRF2 (cat. no. 1254), rabbit mTRF1 (cat. no. 1449), rabbit hTRF2 (cat. no. 647), rabbit hTRF1 (cat. no. 307), mouse PARP1 (Enzo, BML-SA248), mouse PAR (Trevigen, 4335-MC) and rabbit 53BP1 (Abcam ab175933).

FISH on metaphase chromosomes. Telomeric FISH and CO-FISH were conducted as previously described[7,61] with PNA probes (PNA Bio) labeled with Alexa Fluor 647-OO-$(CCCTAA)_3$, Cy3-OO-$(TTAGGG)_3$ or FITC-OO-$(CCCTAA)_3$. Images were captured with a Zeiss Axioplan II microscope equipped with a Hamamatsu C4742-95 camera and controlled by Volocity software (GE Healthcare) and were analyzed with the same software.

For analysis of unequal sister telomeres, the FISH signal intensities of sister telomeres were determined, and local background was subtracted in Volocity software. The ratio of signal intensities between each pair of sister telomeres was calculated (ratio = higher signal/lower signal). In control cells, this 'sister ratio' was expected to be close to 1. To compare different conditions, control cells were used to set a cutoff at the eightieth percentile of sister-telomere ratios. For example, in one particular experiment, the 80% of all sister ratios in the control cells were between 1 and 1.8. For the experimental conditions in the same experiment, sister ratios that exceeded this eightieth-percentile cutoff (i.e., 1.8 in the example) were scored as having unequal sister telomeres. For each experimental condition, 25–45 metaphase spreads from 3 or 4 individual experiments were analyzed, representing a total of 1,000–1,500 pairs of sister telomeres quantified.

For Q-FISH analysis, metaphase spreads were collected and processed as described above, and the TFL-Telo image analysis was used as previously described[62]. At least 15 metaphase spreads were used for analysis of each sample in each experiment. Spreads from HeLa1.3 cells were mixed with the mouse experimental samples and used as internal controls for hybridization efficiency. Telomere fluorescence values from five HeLa1.3 metaphase spreads on each slide were averaged, normalization ratios were calculated, and fluorescence values from experimental samples were subjected to normalization on the basis of these ratios.

Telomeric ChIP. The telomeric ChIP assay was performed as previously described[63]. Telomeric DNA associated with shelterin proteins was immunoprecipitated with anti-rabbit mTRF2 (cat. no.1254), anti-rabbit mTIN2 (cat. no.1447) and protein G magnetic beads (Cell Signaling).

Telomere blots. For telomere-blot analysis of mouse DNA, 0.5×10^6 to 1×10^6 cells were harvested by trypsinization, suspended in PBS, mixed with an equal volume of 2% agarose and cast in plug molds. Cells were digested in the plugs overnight in proteinase K digestion buffer (10 mM Tris-HCl, pH 8.0, 250 mM EDTA, 0.2% sodium deoxycholate, 1% sodium laurylsarcosine and 1 mg/ml proteinase K) at 50 °C. After being washed four times in TE, plugs were incubated with 90 U HindIII or 60 U MboI/AluI (NEB) overnight at 37 °C. Digested DNA was resolved on a 1% agarose/0.5× TBE gel by pulsed-field gel electrophoresis in a CHEF-DRII PFGE apparatus (Bio-Rad). Gel electrophoresis of gDNA from human cells and Southern blotting procedures were performed as previously described[64,65].

For quantification of the telomeric signal from HindIII-digested mouse DNA, a chromosome internal probe was used as loading control (mTRF2 cDNA[14]). The blots were probed with the chromosome-internal probe, stripped with boiling 0.5% SDS/0.1× SSC, rinsed in 2× SSC and then probed with the telomeric probe. For MboI/AluI-digested genomic DNA, a BamHI-repeat probe[53] on a blot containing the smaller restriction fragments was used as a loading reference. For detection of telomeric DNA, the telomere-specific Sty11 probe[66] was used. Uncropped blot images of key data are shown in **Supplementary Data Set 1**.

2D gel electrophoresis. Isolation and digestion of DNA from human cells was performed as described above. Neutral–neutral 2D gel electrophoresis was performed as described previously[14]. 7–12 μg of MboI/AluI-digested genomic DNA was resolved on a 0.4% agarose/1× TBE gel at <1 V/cm for 24 h. The first-dimension gel was stained with 0.3 μg/ml ethidium bromide, and bands were excised and placed 90° relative to the direction of electrophoresis in a 1.1% agarose/1× TBE second-dimension gel supplemented with 0.3 μg/ml ethidium bromide. Electrophoresis was performed for 4 h at 5 V/cm in a cold room. After electrophoresis, the gel was photographed and used for Southern blot analysis as described above.

SCE assay. For the SCE assay, cells were treated with 20 μM BrdU for two cycles of replication. Cells were harvested, and metaphase spreads were prepared as described for telomeric FISH. Sister chromatids were differentially stained with an adapted protocol[67]. Briefly, metaphases were incubated with 25 μg/ml Hoechst 33258 diluted in 2× SSC for 15 min, exposed to UV light (to 5,400 J/m^2), washed in 1× PBS and stained with DAPI in 1× PBS. After dehydration, slides were mounted with ProLong Gold antifade reagent.

Statistical methods. All statistical analysis was performed with GraphPad Prism software. The significance between means was determined by one-way or two-way ANOVA with Tukey post test for multiple comparisons and two-tailed unpaired Student's *t* test when the means of two experimental conditions were compared. The tests used and the number of independent experiments analyzed are indicated in each figure legend. *P* values are as follows: $****P < 0.0001$; $***P < 0.001$; $**P < 0.01$; $*P < 0.05$; and NS, not significant. For key data, *P* values of *t* tests and *F* statistics and degrees of freedom of ANOVAs are reported in **Supplementary Table 1**. Error bars shown represent s.d. or s.e.m. and are defined in the individual figure legends.

A **Life Sciences Reporting Summary** for this paper is available.

Data availability. Primary data are available upon request.

48. Karlseder, J., Smogorzewska, A. & de Lange, T. Senescence induced by altered telomere state, not telomere loss. *Science* **295**, 2446–2449 (2002).
49. Broccoli, D., Smogorzewska, A., Chong, L. & de Lange, T. Human telomeres contain two distinct Myb-related proteins, TRF1 and TRF2. *Nat. Genet.* **17**, 231–235 (1997).
50. Dunderdale, H.J., Sharples, G.J., Lloyd, R.G. & West, S.C. Cloning, overexpression, purification, and characterization of the *Escherichia coli* RuvC Holliday junction resolvase. *J. Biol. Chem.* **269**, 5187–5194 (1994).
51. Frank, K.M. *et al.* Late embryonic lethality and impaired V(D)J recombination in mice lacking DNA ligase IV. *Nature* **396**, 173–177 (1998).
52. Gu, Y. *et al.* Growth retardation and leaky SCID phenotype of Ku70-deficient mice. *Immunity* **7**, 653–665 (1997).
53. Hockemeyer, D., Daniels, J.P., Takai, H. & de Lange, T. Recent expansion of the telomeric complex in rodents: two distinct POT1 proteins protect mouse telomeres. *Cell* **126**, 63–77 (2006).
54. Jacks, T. *et al.* Tumor spectrum analysis in p53-mutant mice. *Curr. Biol.* **4**, 1–7 (1994).
55. Kibe, T., Osawa, G.A., Keegan, C.E. & de Lange, T. Telomere protection by TPP1 is mediated by POT1a and POT1b. *Mol. Cell. Biol.* **30**, 1059–1066 (2010).
56. Nussenzweig, A. *et al.* Requirement for Ku80 in growth and immunoglobulin V(D)J recombination. *Nature* **382**, 551–555 (1996).
57. Takai, K.K., Kibe, T., Donigian, J.R., Frescas, D. & de Lange, T. Telomere protection by TPP1/POT1 requires tethering to TIN2. *Mol. Cell* **44**, 647–659 (2011).
58. Ventura, A. *et al.* Restoration of p53 function leads to tumour regression *in vivo*. *Nature* **445**, 661–665 (2007).
59. Takai, K.K., Hooper, S., Blackwood, S., Gandhi, R. & de Lange, T. *In vivo* stoichiometry of shelterin components. *J. Biol. Chem.* **285**, 1457–1467 (2010).
60. Takai, H., Smogorzewska, A. & de Lange, T. DNA damage foci at dysfunctional telomeres. *Curr. Biol.* **13**, 1549–1556 (2003).
61. Celli, G.B., Denchi, E.L. & de Lange, T. Ku70 stimulates fusion of dysfunctional telomeres yet protects chromosome ends from homologous recombination. *Nat. Cell Biol.* **8**, 885–890 (2006).
62. Poon, S.S. & Lansdorp, P.M. Quantitative fluorescence *in situ* hybridization (Q-FISH). *Curr. Protoc. Cell Biol.* **12**, 18.4 (2001).
63. Loayza, D. & De Lange, T. POT1 as a terminal transducer of TRF1 telomere length control. *Nature* **423**, 1013–1018 (2003).
64. de Lange, T. *et al.* Structure and variability of human chromosome ends. *Mol. Cell. Biol.* **10**, 518–527 (1990).
65. Kabir, S., Hockemeyer, D. & de Lange, T. TALEN gene knockouts reveal no requirement for the conserved human shelterin protein Rap1 in telomere protection and length regulation. *Cell Rep.* **9**, 1273–1280 (2014).
66. de Lange, T. Human telomeres are attached to the nuclear matrix. *EMBO J.* **11**, 717–724 (1992).
67. Bayani, J. & Squire, J.A. Sister chromatid exchange. *Curr. Protoc. Cell Biol.* **25**, 22.7 (2005).

 doi:10.1038/nsmb.3451

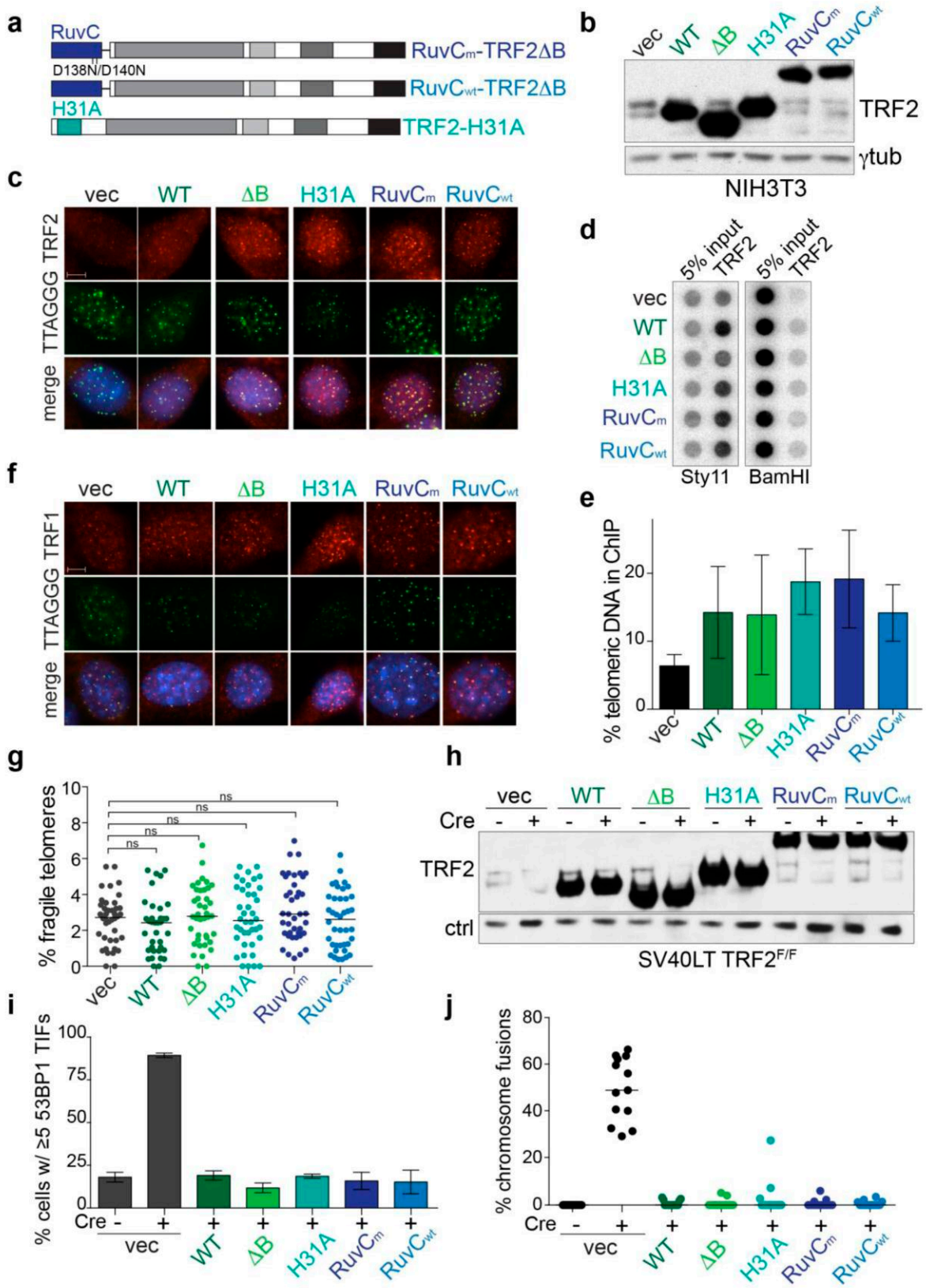

Supplementary Figure 1

Functional analysis of TRF2 alleles.

(**a**) Schematic of RuvC-TRF2ΔB fusion proteins and the TRF2H31A construct. $RuvC_m$ contains mutations in the active site (D138N/D140N) and $RuvC_{wt}$ represents the wild type protein. The mutations in the active site abolish resolvase activity of RuvC but do not affect its binding to branched DNA structures[29]. (**b**) Immunoblot for TRF2 and γ–tubulin in NIH3T3 cells. (**c**) IF-FISH for TRF2 (red) and telomeres (green) in NIH3T3 cells expressing the indicated alleles. Blue, DAPI; Scale bar, 5 μm. (**d**) Telomeric ChIP analysis with TRF2 Ab in NIH3T3 cells expressing the different TRF2 alleles. (**e**) Quantification of telomeric DNA recovered with the TRF2 Ab (average % telomeric DNA recovered in two independent experiments). (**f**) IF-FISH for TRF1 (red) and telomeres (green) in NIH3T3 cells expressing the indicated alleles. Blue, DAPI; Scale bar, 5 μm. (**g**) Analysis of fragile telomeres, a proxy for TRF1 dysfunction, in the indicated NIH3T3 cells. Metaphase chromosomes were prepared five days after introduction of the TRF2 alleles. Data points represent individual metaphases from 3 independent experiments; bars show the median. Significance was calculated by One-way ANOVA with Tukey post-test, ns, not significant. (**h**) Immunoblot showing expression of TRF2 in SV40-LT $TRF2^{F/F}$ MEFs complemented with TRF2 alleles 96 h after Cre. Cre minus cells were harvested at the same time-point. (**i**) 53BP1 TIF analysis in cells as in (h); means±SDs from 3 independent experiments. (**j**) Quantification of telomere fusions in cells as in (h); median fusion frequency in one experiment (13-15 metaphases).

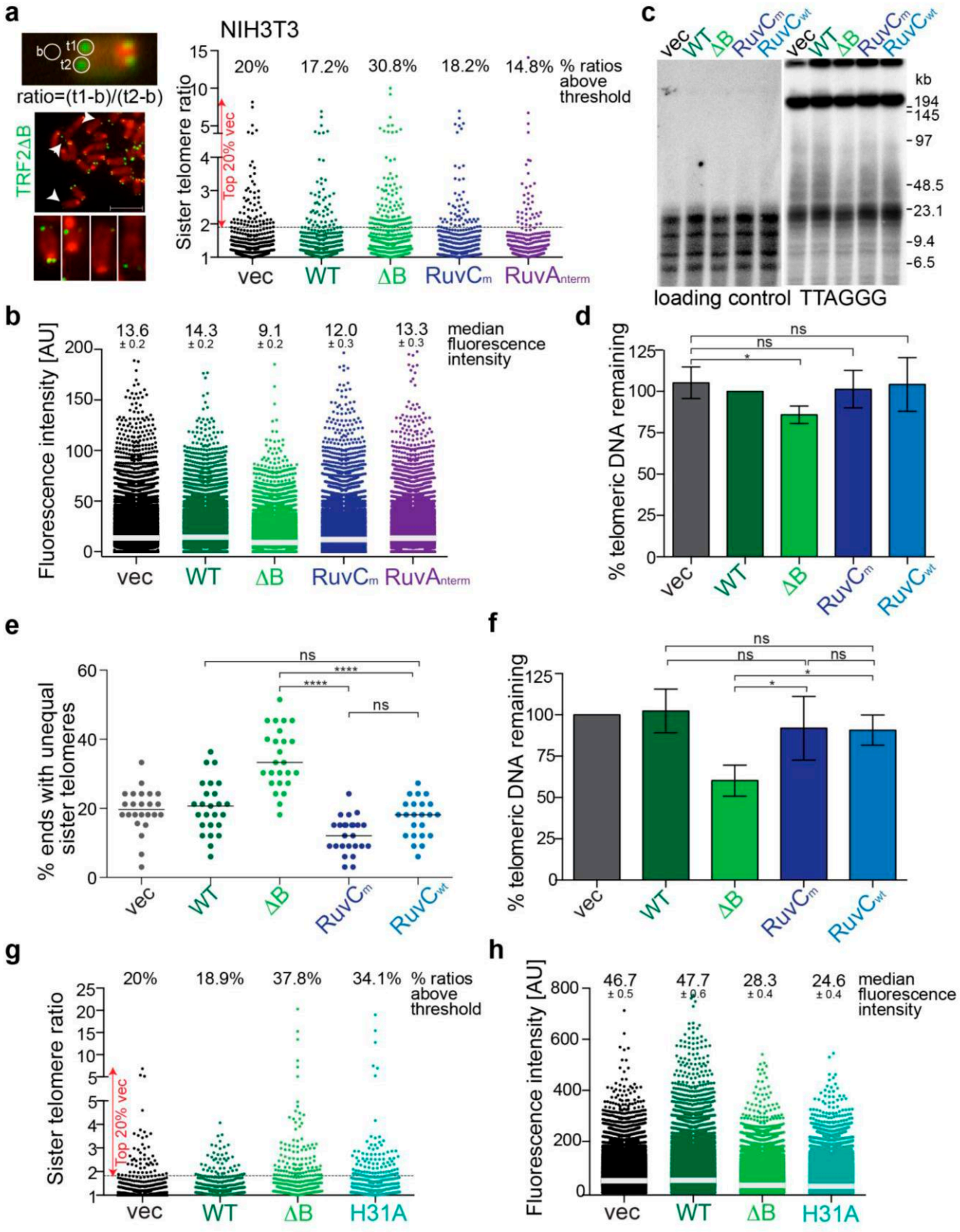

Supplementary Figure 2

RuvA and RuvC protect telomeres in place of the basic domain.

(**a**) Top: Illustration of the approach for measuring unequal sister telomeres. Middle: Representative image showing metaphase chromosomes of TRF2ΔB expressing NIH3T3 cells one day after introduction by retroviral infection. Scale bar, 10 μm. Green: Telomeric FISH; red, DAPI. Arrows: unequal sister telomere signals. Bottom: Enlarged examples of chromosomes with unequal sister telomeres. Right: a scatter plot of the raw sister telomere ratios from one representative experiment is shown. This experiment is part of the analysis of unequal sister telomeres shown in Fig. 2e. Data points represent individual sister ratios (from 330 chromosome ends on 10 metaphase spreads). The dotted line depicts the cut-off used in this experiment to calculate the % of ends with unequal sister telomeres. The cut-off represents the 80^{th} percentile sister ratio in control cells (vec). The scatter plot shows more chromosome ends with a ratio above the threshold in cells expressing TRF2ΔB. The % of ratios above the threshold is indicated. All unequal sister ratios were determined as indicated in (a). (**b**) Scatter plot of raw telomere fluorescence units (TFU in arbitrary units) from Q-FISH analysis in NIH3T3 cells expressing the indicated TRF2 alleles as in Fig. 2f. Median TFU units from 3 independent experiments (medians±SEMs) are indicated (white bars). (**c**) Telomere blot of HindIII-digested DNA from NIH3T3 cells (day 5 post-infection). The membrane was hybridized with a chromosome-internal probe for normalization, stripped, and hybridized to the telomere-specific Sty11 probe to detect telomeric repeats. (**d**) Quantification of telomeric signal intensity, as determined in (c). Telomeric signals were normalized to the signal from the chromosome-internal probe and are shown relative to wt TRF2 (100%). Means±SDs from 6 independent experiments; p-values from One-way Anova with Dunnett's test. (**e**) Quantification of chromosome ends with unequal sister telomeres in NIH3T3 cells. Scatter plots with medians are shown (≥25 metaphases from four independent experiments; p values from One-way ANOVA with Tukey post-test). The same data sets for vec, WT, and ΔB are shown Fig. 2l. (**f**) Q-FISH analysis of telomeric DNA signals in NIH3T3 cells expressing the indicated alleles (% telomeric DNA relative to empty vector; means±SDs from four independent experiments. The same data sets for vec, WT, and ΔB are shown in Fig. 2m. (**g**) Scatter plot of sister telomere ratios from one representative experiment as in Fig. 2l. Data points represent individual sister ratios. This experiment is part of the analysis of unequal sister telomeres shown in Fig. 2l. (**h**) Scatter plot of raw TFUs from Q-FISH analysis in NIH3T3 cells expressing the indicated TRF2 alleles as in Fig. 2m. Median TFU units from 5 independent experiments (medians±SEMs) are indicated (white bars).

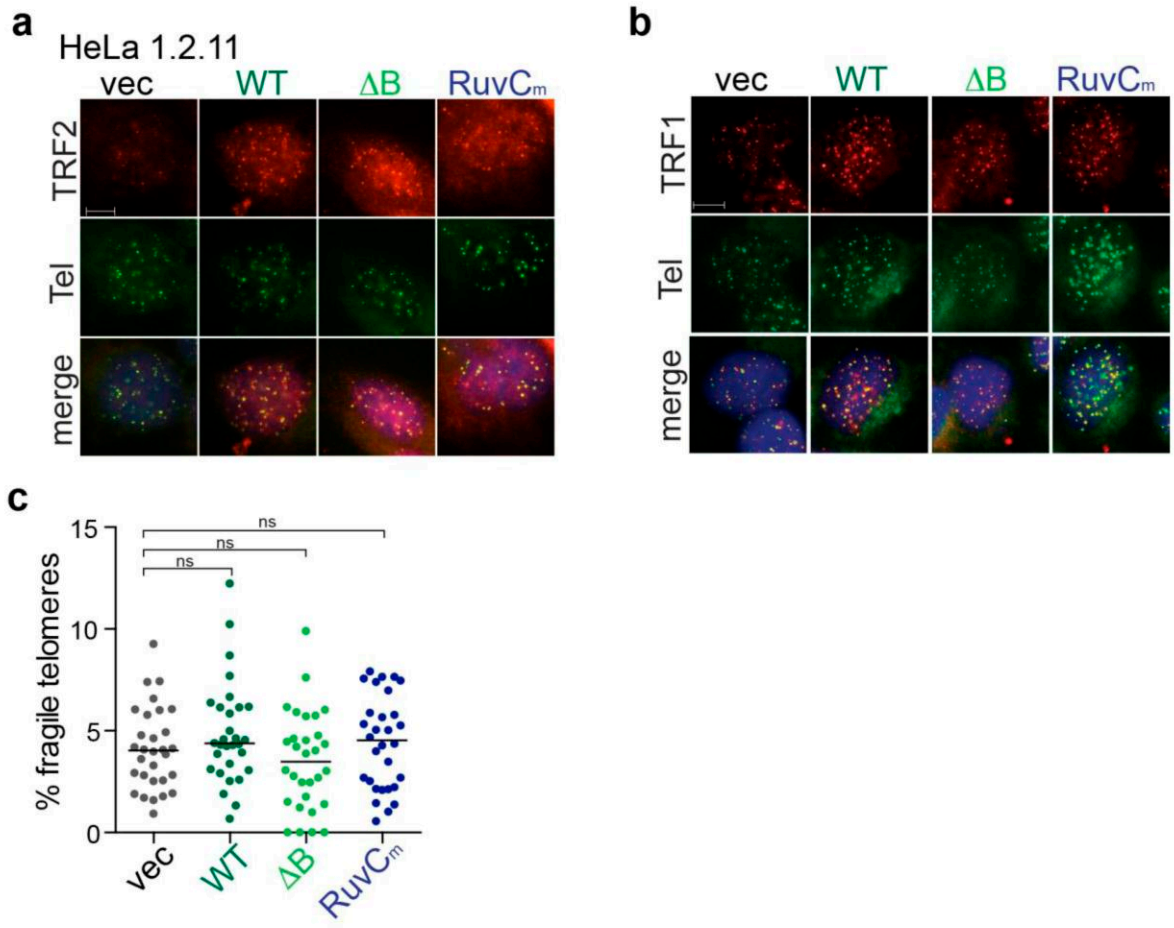

Supplementary Figure 3

Control experiments on HeLa cells.

(**a**) IF-FISH to detect TRF2 (red) and telomeres (green) in HeLa1.2.11 cells (Day 8 post-infection). Blue, DAPI; Scale bar, 5 μm. (**b**) IF-FISH to detect TRF1 (red) and telomeres (green) in HeLa1.2.11 cells as in (a). TRF1 localization to telomeres is not affected by overexpression of TRF2 alleles. Blue, DAPI; Scale bar, 5 μm. (**c**) Quantification of chromosome ends with fragile telomeres, a proxy for TRF1 function in HeLa1.2.11 cells as in (a). The analysis shows that similar to mouse telomeres, expression of TRF2 alleles does not induce fragile telomeres. Data points represent individual metaphases from 3 independent experiments and significance is based on One-way ANOVA with Tukey post-test as in Fig. 1. Bars represent the median.

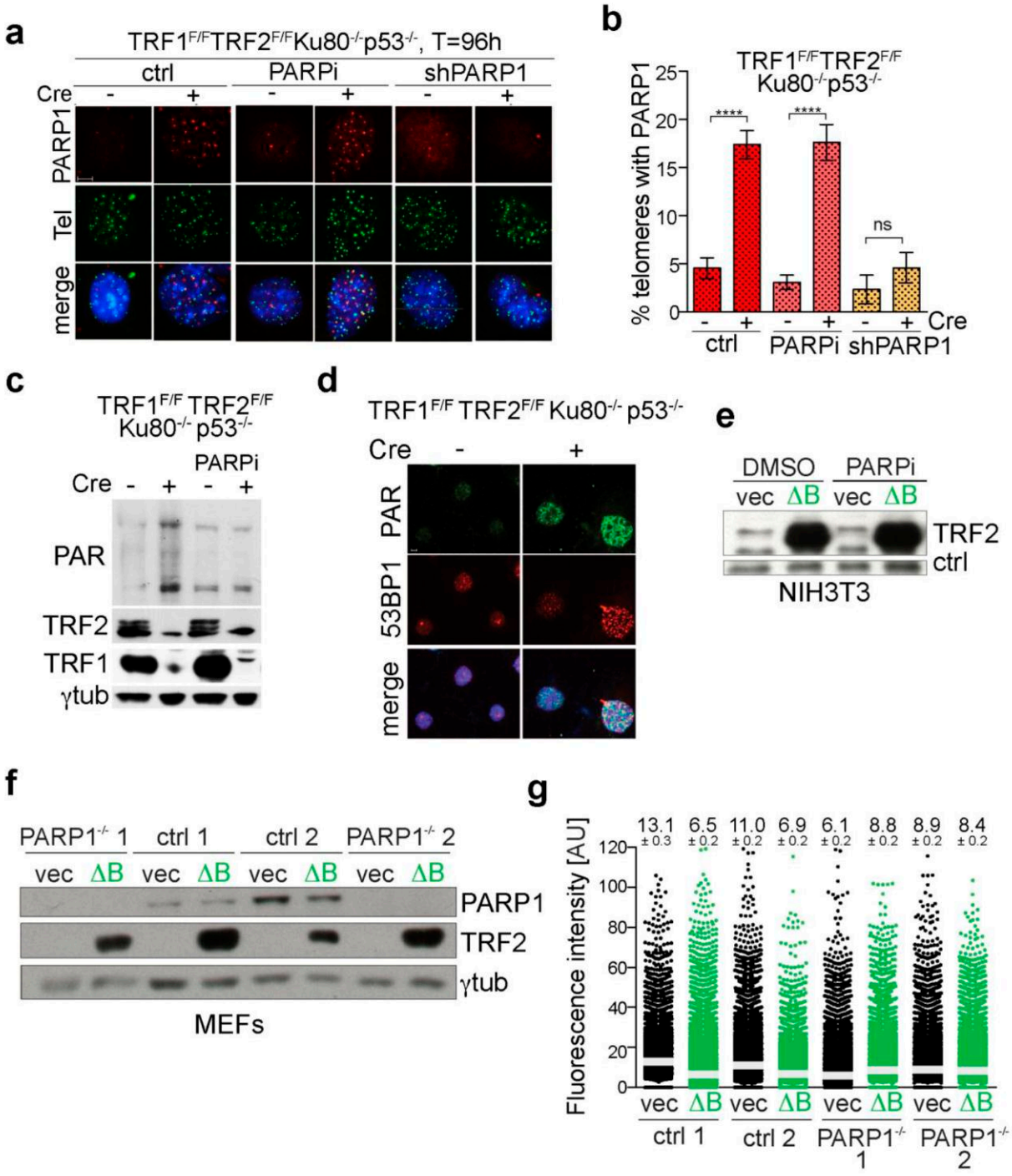

Supplementary Figure 4

TRF2ΔB-induced telomere loss depends on PARP1.

(**a**) Detection of PARP1 and telomeres in TRF1$^{F/F}$TRF2$^{F/F}$Ku80$^{-/-}$p53$^{-/-}$ MEFs with and without Cre (96 h). Red, IF for PARP1; green, telomeric FISH; blue, DAPI. Scale bar, 5 μm. (**b**) Quantification of PARP1 signals co-localizing with telomeres as assessed by IF-FISH in TRF1$^{F/F}$TRF2$^{F/F}$Ku80$^{-/-}$p53$^{-/-}$ MEFs with and without Cre treatment as in (a) (means±SDs from 3 independent experiments; Colocalization was assessed in 40-50 nuclei per experiment and experimental condition; p values from One-way ANOVA with Tukey post test). (**c**) Immunoblot showing TRF2 and TRF1 loss, and induction of PARsylation upon Cre treatment of TRF1$^{F/F}$TRF2$^{F/F}$Ku80$^{-/-}$p53$^{-/-}$ cells. Treatment with 5 μM Olaparib (PARPi) verifies PARP1 dependent PARsylation. (**d**) IF for PAR (green) in

$TRF1^{F/F}TRF2^{F/F}Ku80^{-/-}p53^{-/-}$ cells. Dysfunctional telomeres are visualized by 53BP1 IF (red). Blue, DAPI; Scale bar, 5 μm. (**e**) Immunoblot showing TRF2 in control and TRF2ΔB-expressing NIH3T3 cells that were mock treated (DMSO) or treated with 2 μM Olaparib (PARPi). (**f**) Immunoblot showing TRF2ΔB expression in PARP1-proficient and -deficient MEFs infected with empty vector or TRF2ΔB. Control cell lines were $PARP1^{wt/-}$ (ctrl1) and $PARP1^{wt/wt}$ (ctrl2). (**g**) Scatter plot of telomere fluorescence units (TFU) from Q-FISH analysis in PARP1-proficient and -deficient MEFs infected with vec or TRF2ΔB as in (f). TFU units from 2 independent experiments (medians±SEMs) are shown (white bars).

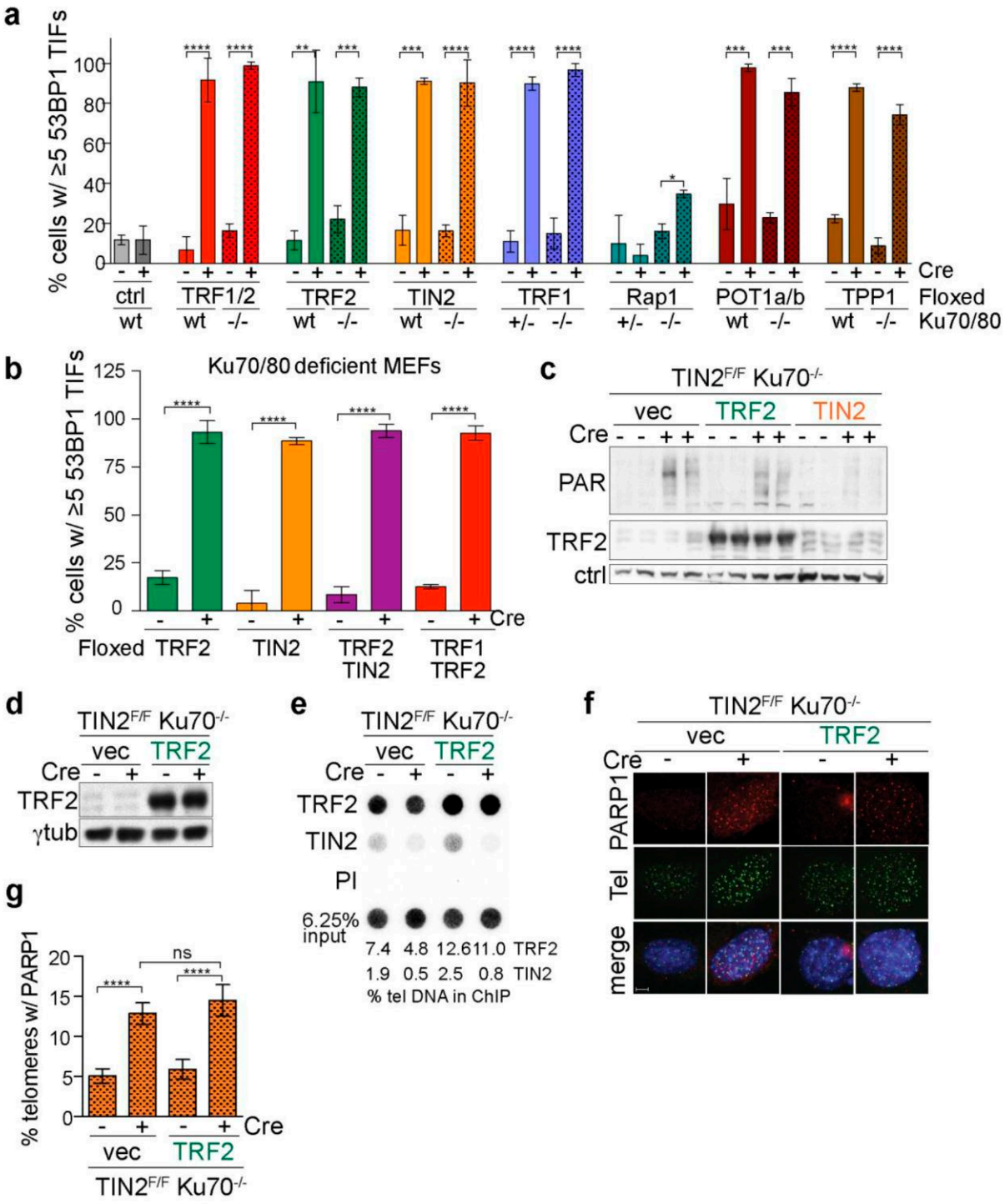

Supplementary Figure 5

TRF2 and TIN2 independently repress telomeric PARP1 signaling.

(**a**) Quantification of cells with ≥5 53BP1 TIFs in the indicated conditional KO MEFs (Cre minus and plus; means±SDs from ≥3 independent experiments). 53BP1 TIF analysis serves as a control for efficient deletion of shelterin components in the survey of MEF cell lines for PARP1 activation. Note that deletion of Rap1 does not induce TIFs in Ku-proficient cells and only to a minor level in Ku-deficient cells. Efficient deletion was also verified by immunoblot analysis using specific antibodies for the individual shelterin subunits. (**b**) Quantification of cells with ≥5 53BP1 TIFs in cells as in Fig. 4b (Cre minus and plus; means±SDs from 3 independent experiments).

53BP1 TIF analysis was used to control for efficient deletion of shelterin components. Efficient deletion was also verified by immunoblot analysis using specific antibodies for the individual shelterin subunits (**c**) Immunoblot showing PAR and TRF2 in $TIN2^{F/F}Ku70^{-/-}$ MEFs. Note that PARsylation was rescued by expression of TIN2, but not expression of TRF2. (**d**) Immunoblot showing TRF2 overexpression in $TIN2^{F/F}Ku70^{-/-}$ MEFs. (**e**) Telomeric ChIP for TRF2 and TIN2 in $TIN2^{F/F}Ku70^{-/-}$ MEFs. The quantification shows that TRF2 overexpression re-establishes the telomeric TRF2 levels in TIN2/Ku70 DKO cells. (**f**) IF-FISH for PARP1 (red) and telomeres (green) in cells as in (d); DAPI (blue); Scale bar, 5 μm. (**g**) Quantification of PARP1 co-localization with telomeres as in (f) (means±SDs from 3 independent experiments). All experiments were performed at 96 h after Cre. For all experiments, P values are as in Fig. 1 based on One-way ANOVA with Tukey post-test.

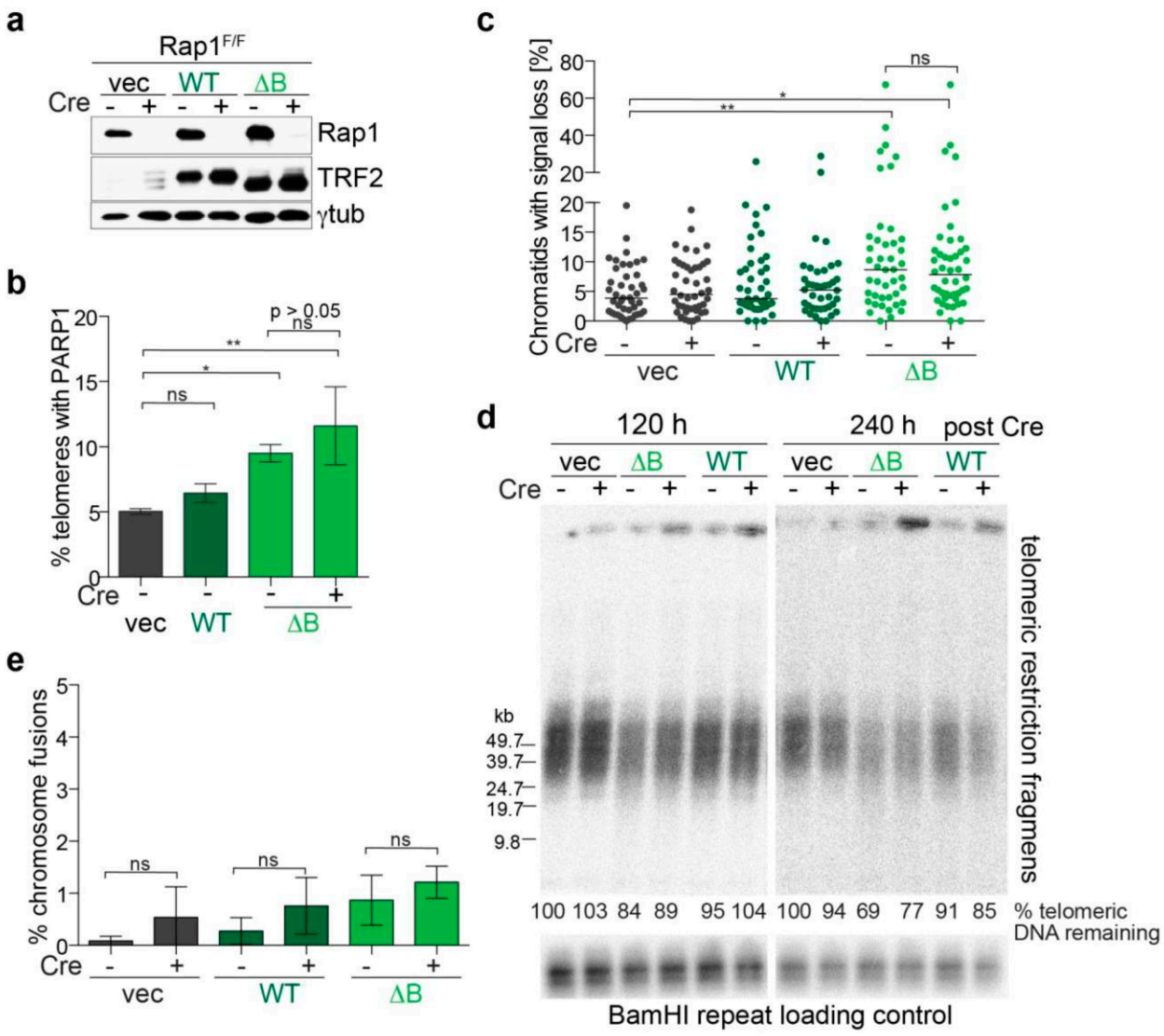

Supplementary Figure 6

Rap1 deletion does not exacerbate phenotypes associated with telomeres containing TRF2ΔB.

(**a**) Immunoblot showing TRF2 alleles and Rap1 in Rap1$^{F/F}$ Ku70$^{+/-}$ p53$^{-/-}$ MEFs with and without Cre treatment. Cells were infected with TRF2 alleles and selected for integration of the TRF2 expression plasmid for 4-5 days. Then the cells were split, H&R Cre infected and harvested 120h post Cre treatment. This experimental setting allows the analysis of the effect of Rap1 deletion on TRF2ΔB-induced phenotypes in an isogenic background. (**b**) Quantification of PARP1 signals co-localizing with telomeres as assessed by IF-FISH in Rap1$^{F/F}$ Ku70$^{+/-}$ p53$^{-/-}$ MEFs as in (a) (means±SDs from 3 independent experiments, P values are based on One-way ANOVA with Tukey post-test). (**c**) Quantification of chromatids that do not have detectable telomere FISH signal in Rap1$^{F/F}$ Ku70$^{+/-}$ p53$^{-/-}$ MEFs as in (a). Scatter plots with medians are shown (≥40 metaphases from three independent experiments; p values from One-way ANOVA with Tukey post-test.) (**d**) Telomere blot analysis of MboI/AluI-digested DNA from Rap1$^{F/F}$ Ku70$^{+/-}$ p53$^{-/-}$ MEFs expressing the indicated TRF2 alleles with or without Cre treatment. Cells were harvested 120h (left panels) or 240h (right panels) post Cre treatment. The lower panels show the signal detected with the BamHI probe, which serves as loading control. The relative telomere abundance calculated from the telomere blot and normalized to the BamHI signal is indicated. The signal in Cre minus control cells was set to 100% for each time point. This panel shows a representative blot. The experiment was repeated 3 times. (**e**) Quantification of chromosome fusions that do not have detectable telomere signals at the fusion sites in Rap1$^{F/F}$ Ku70$^{+/-}$ p53$^{-/-}$ MEFs as in (a) (means±SDs from 3 independent experiments, ≥40 metaphase spreads, p-values from unpaired t-test). P value symbols are as in Fig.1.

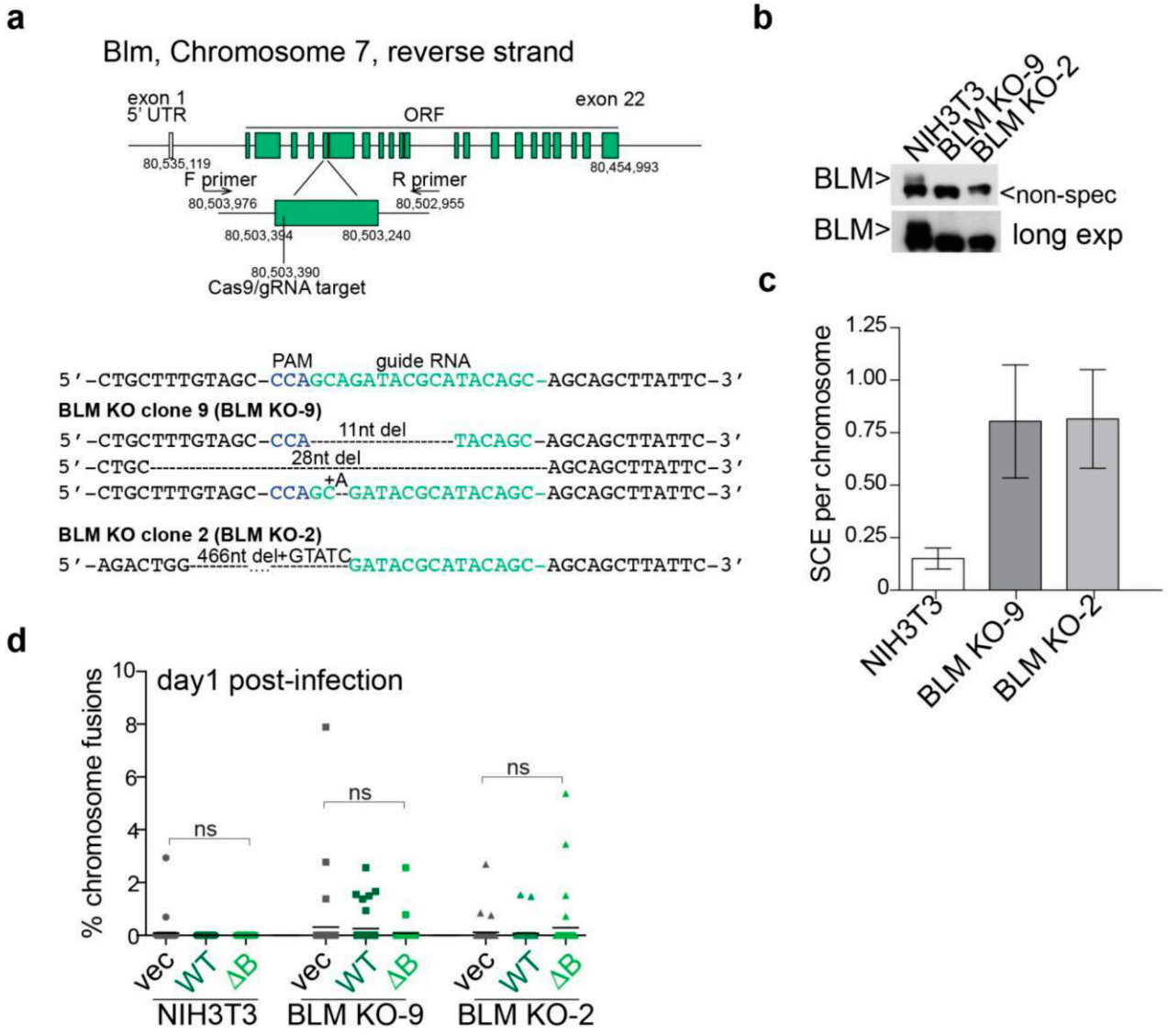

Supplementary Figure 7

Generation of BLM-KO cells by CRISPR–Cas9 gene editing.

(**a**) Schematic of the BLM locus showing landmarks relevant to CRISPR/Cas9 gene editing. The guide RNA (gRNA) region and the PAM are indicated in the reference sequence and the changes in sequence are highlighted in the edited alleles of the two CRISPR clones. In clone BLM KO-2 only one allele variant (and no wt allele) was detected. The sequences were derived from TOPO-cloned PCR products amplified from the indicated primer pair. (**b**) Immunoblot showing BLM (arrow) in parental NIH3T3 cells but not in the KO clones. (**c**) SCE assay in parental NIH3T3 cells and the two BLM KO clones confirming BLM deficiency. (**d**) Quantification of chromosome fusions that do not have detectable telomere signals at the fusion sites in parental and BLM KO NIH3T3 cells on day 1 after infection. Dots represent the % of fused chromosomes in individual metaphase spreads and the mean is shown (40 metaphase spreads from 4 independent experiments. P values are as in Fig. 1 based on One-way ANOVA with Tukey post-test.

Figure	Statistical test used		F (DFn, DFd)
Fig. 1g	One-way ANOVA		F (2, 6) = 11.02
Fig. 1j	One-way ANOVA		F (2, 6) = 183.9
Fig. 1k	unpaired - two tailed t-test		p= 0.2740
Fig. 2d	One-way ANOVA		F (2, 6) = 292.4
Fig. 2e	One-way ANOVA		F (4, 161) = 20.29
Fig. 2f	One-way ANOVA		F (4, 10) = 4.415
Fig. 2h	One-way ANOVA		F (3, 124) = 16.36
Fig. 2l	One-way ANOVA		F (3, 95) = 31.50
Fig. 2m	One-way ANOVA		F (3, 16) = 23.75
Fig. 3a	One-way ANOVA		F (3, 117) = 15.46
Fig. 3b	One-way ANOVA		F (3, 231) = 24.61
Fig. 3c	One-way ANOVA		F (3, 12) = 7.500
Fig. 3f	One-way ANOVA		F (5, 12) = 92.98
Fig. 4a	One-way ANOVA		F (29, 96) = 37.38
Fig. 4c	One-way ANOVA		F (7, 16) = 58.45
Fig. 4d	One-way ANOVA		F (3, 116) = 12.86
Fig. 5b	Two-way ANOVA	Interaction	F (4, 473) = 1.541
		TRF2 allele	F (2, 473) = 106.9
		Genotype	F (2, 473) = 5.777
Fig. 5d	Two-way ANOVA	Interaction	F (4, 470) = 7.117
		TRF2 allele	F (2, 470) = 67.98
		Genotype	F (2, 470) = 11.62
Fig. 5e	One-way ANOVA		F (8, 470) = 23.78
Fig. 5f	Two-way ANOVA	Interaction	F (4, 610) = 2.028
		TRF2 allele	F (2, 610) = 26.46
		Genotype	F (2, 610) = 10.23
Fig. 6b	One-way ANOVA		F (4, 296) = 10.32
Fig. 6d	One-way ANOVA		F (3, 263) = 5.501

Supplementary Table 1

F statistics and degrees of freedom of ANOVAs.